Universitat Politècnica de Catalunya

Neuronal encoding and transmission of weak periodic signals

Maria Masoliver Vila

A thesis submitted in fulfillment of the requirements for the degree of Doctor in Computational and Applied Physics

SUPERVISOR Cristina Masoller

January 2020

Emmarco amb quatre fustes
un pany de cel i el penjo a la paret.

Jo tinc un nom
i amb guix l'escric a sota.

Divisa
Maria-Mercè Marçal

Abstract

Sensory neurons use sequences of electrical pulses (known as action potentials or spikes) to encode and transmit information of external temporal stimuli. Neural coding is the research field that studies the relationship between external stimuli and neuronal responses. Since there is not a unique relationship between them, the mechanisms underlying neural coding are not yet fully understood. However, it is known that neurons use different mechanisms to encode external stimuli, which can be complementary or functional under different situations. An important issue is how neural noise (stochastic electrical fluctuations which do not carry any information) influences neural coding. Here we focus on the response of noisy neurons to a weak and periodic external input. The signal is considered weak enough to be sub-threshold, i.e., by itself it does not induce spikes. However, neural noise triggers spikes, which encode the information of the weak signal. In this situation a encoding mechanism based on symbolic spike patterns has been been proposed for single (uncoupled) neurons; here we aim to determine if this mechanism is plausible for coupled neurons.

First, we use the FitzHugh-Nagumo model to study two coupled neurons. We consider the situation in which only one neuron perceives the weak signal (named as neuron 1). We characterize the role of the coupling on the encoding of the signal and we analyze the sequences of inter-spike-intervals of neuron 1 using the symbolic method (known as ordinal analysis), which can capture preferred and infrequent spike patterns (defined by the time interval between spikes). Indeed, we demonstrate that the encoding mechanism is robust to coupling: the neuron that perceives the signal fires a spike train

that has preferred and infrequent spike patterns which carry information about the signal's amplitude and frequency.

Second, we apply ordinal analysis to the sequences of inter-spike-intervals generated by two coupled Morris-Lecar neurons. We investigate if different neuron types (regarding class 1 or class 2 excitability) generate similar spike sequences, and characterize the differences in signal encoding and transmission when changing the type of coupling (electrical or excitatory chemical synapses). We find that depending on the signal frequency, specific combinations of neuron/class and coupling type allow a more effective encoding, or a more effective transmission of the signal.

Third, we analyze the activity of an ensemble of neurons, when they all perceive the weak signal. We apply ordinal analysis to the spike sequences of all neurons and we demonstrate that a neuronal ensemble can also encode information of the signal in the form of preferred or infrequent spikes patterns, as one or two coupled neurons do. Also, we show that neuronal coupling is beneficial for signal encoding (because the neuronal ensemble detects signals of weaker amplitude) and that just few links among neurons can significantly improve signal encoding (because the probabilities of the preferred and the infrequent patterns take extremer values).

Taken together, the results presented in this thesis suggest that a temporal code based not on the precise timing but on the relative timing of the spikes of individual neurons is a plausible mechanism for encoding the information of weak periodic external stimuli.

Resum

Les neurones sensorials disparen seqüències d'impulsos elèctrics (coneguts com a potencials d'acció) per codificar i transmetre informació d'estímuls temporals externs. La codificació neuronal és el camp d'investigació que estudia la relació entre els estímuls externs i les respostes neuronals. Atès que no hi ha una relació única entre ells, els mecanismes subjacents a la codificació neural encara no es comprenen plenament. No obstant això, se sap que les neurones utilitzen diferents mecanismes per codificar els estímuls externs, que poden ser complementaris en diferents situacions. Una qüestió important és com el soroll neuronal (fluctuacions elèctriques estocàstiques que no transmeten cap informació) influeix en la codificació neuronal.

Aquí ens centrem en com les neurones responen a un senyal feble i periòdic. El senyal es considera prou feble com per ser subumbral, és a dir, per si sol no indueix a les neurones a disparar. No obstant això, el soroll neuronal desencadena potencials d'acció que codifiquen la informació del senyal feble. En aquesta situació s'ha proposat un mecanisme de codificació basat en patrons simbòlics per a neurones desacoblades; en aquesta tesis tractarem de determinar si aquest mecanisme és plausible per a neurones acoblades.

Hem fet servir, primerament, el model neuronal Fitzhugh-Nagumo per estudiar dues neurones acoblades. Hem considerat la situació en la qual només una neurona percep el senyal feble (l'anomanem neurona 1). Hem caracteritzat el paper de l'acoblament en la codificació del senyal i hem analitzat les seqüències d'intervals entre potencials d'acció de la neurona 1 utilitzant el mètode *anàlisi simbòlic*, el qual pot capturar patrons d'impulsos elèctrics preferits i infreqüents (definits pel

temps relatiu entre impulsos). De fet, hem demostrat que el mecanisme de codificació és robust a l'acoblament: la neurona que percep el senyal dispara una seqüència d'impulsos elèctrics, la qual conté patrons preferits i infreqüents que depenen de l'amplitud i freqüència del senyal.

En segon lloc, hem aplicat l'anàlisi simbòlic a les seqüències d'intervals entre potencials d'acció generats per dues neurones acoblades simulades amb el model neuronal Morris-lecar. Hem investigat si diferents tipus de neurones (pel que fa al tipus d'excitabilitat neuronal, classe 1 o classe 2) generen seqüències de potencials d'acció similars, i hem caracteritzat les diferències en la codificació i transmissió del senyal en canviar el tipus d'acoblament (sinapsis elèctriques o químiques excitatòries). Podem establir que depenent de la freqüència del senyal, combinacions específiques de neurona/classe i tipus d'acoblament permeten una codificació més efectiva, o una transmissió més efectiva del senyal.

En últim lloc, hem analitzat l'activitat d'un conjunt de neurones, quan totes elles perceben el senyal feble. L'anàlisi simbòlic l'hem aplicat a les seqüències d'accions de potencials de totes les neurones i hem demostrat que un conjunt neuronal també codifica la informació del senyal en forma de patrons d'accions de potencials preferits o poc freqüents, com ho fan una sola o dues neurones acoblades. A més, hem establert que l'acoblament neuronal és beneficiós per a la codificació de senyals (ja que el conjunt neuronal detecta senyals d'amplitud més febles) i que amb només pocs enllaços entre neurones podem millorar significativament la codificació de senyals (ja que les probabilitats dels patrons preferits i dels poc freqüents prenen valors més extrems).

En conjunt, els resultats presentats en aquesta tesi suggereixen que un codi neuronal temporal basat no en el temps precís sinó en el temps relatiu dels potencials d'acció de les neurones individuals és un mecanisme plausible per codificar la informació dels estímuls externs periòdics febles.

Agraïments

Són moltes les persones que han contribuït d'una manera o una altra a la realització i finalització d'aquesta tesis. M'agradaria agraïr especialment a la Cristina Masoller, que és qui em va donar la oportunitat de treballar al grup de recerca de dinàmica no lineal, òptica no lineal i làsers (DONLL) i al llarg d'aquests tres anys m'ha guiat i aconsellat per dur-la a terme. Als altres investigadors del grup, al Kestas Staliunas, a la Muriel Botey, al Ramon Herrero, al Ramon Vilaseca, a la Crina Cojocaru i al Toni Pons. Al Jordi Tiana i al Carlos Quintero per les numeroses discusions, dubtes computacionals, problemes burocràtics variats que m'han ajudat a resoldre. Als companys de grup, a la Judith, al Shubham, al Donatus, al Pablo, al Dario, al Hossam, a la Laura i al Salim. I especialment al Riccardo, que l'he empipat més del que hagués volgut amb dubtes de neurosciència. També al Fabián, a la Concetta i al Tetsu. Al Claudio Mirasso i al Cristian Estarellas, per poder col·laborar amb ells i sentir-me com a casa a l'IFISC. Moltes gràcies al meu tiet Marc Castells, que ha disenyat la portada i m'ha donat molts bons consells per la maquetació de la tesis. M'agradaria donar les gràcies també a aquells amics fora de l'òrbita científica que m'han recolzat al llarg d'aquests tres anys i han viatjat amb mi en el meu tren emocional: al Gerard, a la Laia, a la Clara, a la Gemma, la Marina, a la Núria, a la Sanjukta, a la Maria, la Lucía i a la Carlota. A l'Oleguer, a la Mar, a l'Andrea i al Matteo per fer del pis una casa. Especialment al Matteo per cuidar-me en aquest últim període. A les sardines, clarament. I finalment, als meus pares, al meu germà i a l'Anna, que m'han recoltzat en tot el que m'he proposat i han fet possible que ho aconseguís.

Contents

Abstract **v**

Resum **viii**

Agraïments **xii**

1 Introduction **1**
1.1 Neuronal dynamics 1
1.1.1 Neuronal excitability 5
1.1.2 Neural noise 8
1.2 Neural coding 9
1.3 Objectives and outline of the thesis 16

2 Models and methods **19**
2.1 Models 19
2.1.1 FitzHugh-Nagumo model 21
2.1.2 Morris-Lecar model 23
2.1.3 Model simulations and spike detection . 25
2.2 Time-series analysis of spike sequences 26
2.2.1 Spike regularity 26
2.2.2 Ordinal analysis 27
2.2.3 Synchronization measures 31

3 Signal encoding and transmission by two FitzHugh-Nagumo neurons 35
3.1 Sub-threshold region in the parameter space (a_o, T) 37
3.2 Influence of coupling coefficients on the spike rate 40
3.3 Influence of noise and modulation parameters on the spike rate 41
3.4 Detection and characterization of spike patterns 45
3.4.1 Analysis of two coupled non-identical neurons 51
3.4.2 Signal transmission 54
3.5 Discussion 59

4 Signal encoding and transmission by two Morris-Lecar neurons 61
4.1 Signal encoding 66
4.2 Signal transmission 72
4.3 Discussion 75

5 Ensemble of FitzHugh-Nagumo neurons 77
5.1 Influence of the signal's amplitude and frequency 79
5.2 Influence of noise strength 84
5.3 Influence of the network structure 85
5.4 Discussion 88

6 Conclusions and Perspectives 91
6.1 Conclusions 91
6.2 Future perspectives 94

A List of publications and research activities 97

Chapter 1

Introduction

1.1 Neuronal dynamics

The nervous system regulates and controls the activity and functions of the body through the central nervous system and the peripheral nervous system. The peripheral nervous system connects through nerves (bundles of long fibers) the central nervous system to organs and limbs. The central nervous system processes external and internal information and coordinates the activity of all parts of the body. The two main parts of the central nervous system are the brain and the spinal cord. The brain controls motor and sensory functions (such as eye movement after a visual stimuli) and it performs high cognitive functions (such as language processing, reasoning or memory tasks). On the other hand, the spinal cord is responsible for carrying signals from the brain to other parts of the body and vice versa, it is responsible for many of our quick and involuntary reflexes and it also controls movements of the limbs and the trunk.[1]

Neurons are the fundamental units of the brain and the spinal cord. Camilo Golgi (1843-1926) and Santiago Ramón y Cajal (1852-1934) gave the first detailed descriptions of neurons. In particular, Golgi developed a method of staining nervous tissue (called Golgi's method) which allowed to observe in detail the morphology of individual neurons. Besides, Ramón

y Cajal studied and later described the morphology of neurons (see Fig. 1.1). He was one of the first scientists that defended the neuron doctrine, which states that neurons are the anatomical, physiological, genetic and metabolic units of the nervous system.[2,3] Golgi and Ramón y Cajal jointly received the Nobel Prize in Physiology of Medicine in 1906 *in recognition of their work on the structure of the nervous system.*

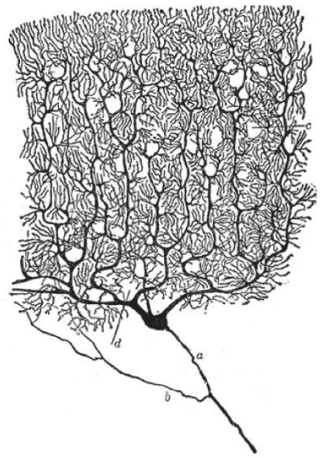

Figure 1.1: Drawing of a Purkinje cell of an adult man by Ramón y Cajal. Purkinje cell is a neuron located in the cerebellum (part of the human brain). From.[3]

A neuron has three differentiated regions: the dendrites, the soma and the axon (see Fig. 1.2). Dendrites are the extensions of the neural cell that receive electrical signals from other neurons and propagate to the cell body, i.e., the soma, of the neuron. The axon is the part of the neuron that propagates electrical signals from the cell body to the dendrites of other neurons. These electrical signals are called action potentials (or spikes) and are the language neurons use to communicate among them: once a neuron fires an action potential (due to

an external stimuli or due to an action potential of another neuron), it might elicit, in turn the generation of another action potential in another neuron.

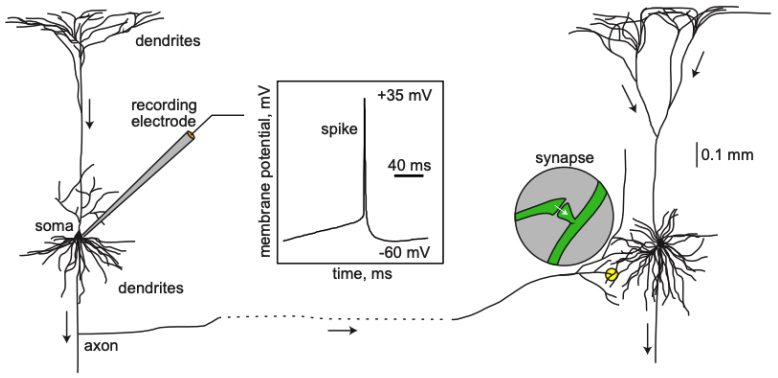

Figure 1.2: Structure of a neuron: the dendrites, the soma and the axon. A neuron is connected to other neurons via a synapse. The inset shows an example of an action potential. From.[4]

There are many types of neurons (regarding morphology, physiology, function and dynamics) both in the brain and the spinal cord. While in the brain the distinction between types of neurons is quite complex, in the spinal cord is straightforward; we can easily differentiate three types of neurons regarding their functionality: sensory neurons, motor neurons and interneurons. Sensory neurons are sensitive to external perturbations: they fire an action potential to the central nervous system when they receive sensory input from the environment, motor neurons control our muscle movements and glandular output by transmitting action potentials from the central nervous system and interneurons connect neurons to one another: they transmit electrical signals from motor neurons to sensory ones.[5]

Between two neurons there is a gap called synapse, which is responsible for signal transmission. Each neuron has approximately 10.000 synapses, but some may have up to 150.000. Synapses pass a signal from one neuron (presynaptic) to the next neuron (postsynaptic). Synapses can be electrical or chemical.[6]

Electrical synapses

Electrical synapses directly connect through gap junctions[a] the citoplasm of the presynaptic neuron to the citoplasm of the postsynaptic one, which allows electrical current to pass in both directions.[6] Yet, in some cases electrical synapses are not bidirectional symmetric: the efficacy of transmission in one direction is lower than in the other one; as for example, the giant motor synapse of the crayfish.[7] Electrical synapses allow for a rapid and bidirectional conduction of electrical signals from neuron to neuron, which easily synchronizes the activity among connected neurons.[7]

Chemical synapses

Chemical synapses are synapses that use chemical messengers (known as neurotransmitters) to transmit signals from a presynaptic neuron to a postsynaptic neuron. When an action potential arrives at the synapse it leads to the release of a neurotransmitter, which binds to receptors located in the membrane of the postsynaptic neuron. In turn, ion channels open and allow the flow of ions into the postsynaptic cell. The

[a] Gap junctions are inter-cellular connections that establish a bidirectional communication between cells by allowing small molecules, ions or electrical impulses to pass through a regulated gate between cells. They occur in almost all animal cells that touch each other.

ion flow can be positively or negatively charged, thus chemical synapses can have either an excitatory effect (i.e., depolarizing effect: positive flow of ions into the neuron) or an inhibitory effect (i.e., hyperpolarizing effect: negative flow of ions into the neuron) on the postsynaptic neuron.[8]

1.1.1 Neuronal excitability

Action potentials are the result of the excitability of neurons. Excitability is characteristic of many systems in nature: cardiac tissues, chemical reactions and ion channels, to mention just a few examples.[9] Three states describe the dynamics of excitable systems: a rest state, an excited state and a refractory state. Excitable systems have a well-defined threshold. The system can only perform a particular action (i.e., leave the rest state and go through the excited state) for a sufficiently strong external perturbation which allows the system to exceed the threshold, otherwise for small perturbations the system responds with small damped oscillations (i.e., subthreshold oscillations). After the system performs the action, it needs some time to be ready to perform a second action in response to a second stimulus. This time is known as the refractory period: the system resides in the refractory state. If a second stimulus arrives during the refractory time, the system is incapable of repeating the action. An important characteristic of an excitable system is that the strength of the system's response is independent of the strength of the stimulus.

In the case of a neuron, the resting state of the membrane potential is about -70 mV (relative to the surrounding extracellular medium, which is defined to be 0 mV). In order to support this membrane potential difference, there are ion pumps all along the cell membrane which keep potential concentra-

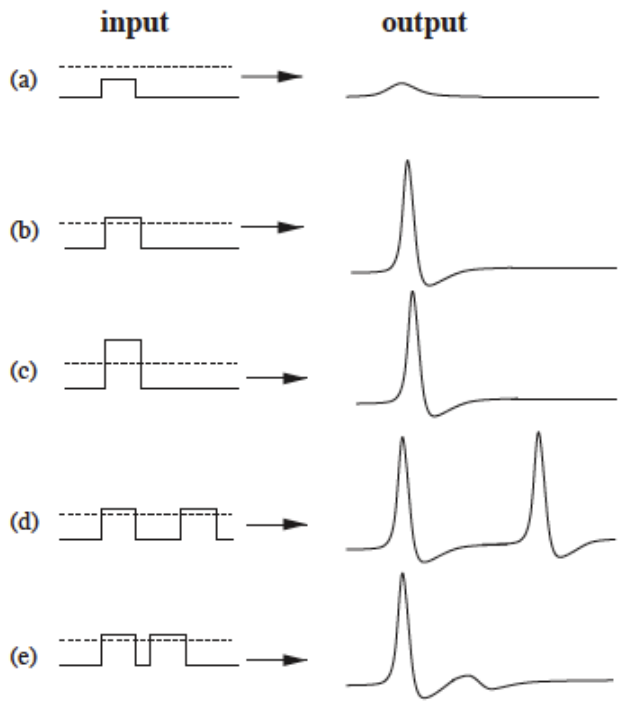

Figure 1.3: The different states of a neuron's excitability. (a) An input below the threshold results in small oscillations around the system's stable state; (b) and (c) an input above the threshold (no matter its amplitude) results in a spike; (d) a second stimulus can lead to a second spike if it takes place after the system's refractory period; (e) if the second stimulus takes place right after a previous stimulus, the neuron will not respond. From.[9]

tion gradients. For example, there is a larger concentration of K+ inside the neuron than in the extracellular medium, on the other hand, Na+ concentration is much higher outside than inside the neuron.[8] When small perturbations arrive (i.e., flow of ions in and out of the neuron) the membrane potential can rise or decrease, performing damped oscillations around the rest state [Fig. 1.3(a)] . If the perturbation is large enough (large influx of positive ions inside the neuron) the membrane

potential rapidly rises (depolarization of the cell) and falls (hyperpolarization of the cell); performing the action potential, a process that is schematically shown in Fig. 1.3(b).

The amplitude of the action potential does not depend on the strength of the stimulus [Fig. 1.3(c)]. The neuron needs some time before it can fire another action potential [Fig. 1.3(d) and (e)].

While all neurons are excitable, the response to an external input varies from neuron to neuron. Two neurons can be morphological identical but they might respond differently to a same synaptic input because of each cell's intrinsic state and properties.[10] Indeed, Hodgkin (1948)[11] injected a DC-current to isolated axons from the same crustacean *Carcinus maenas* and found out that while some of them responded to inputs of arbitrarily low frequency with sustained spikes sensitive to the input frequency, others responded only to inputs of larger frequencies with sustained spikes in a certain frequency band.[4]

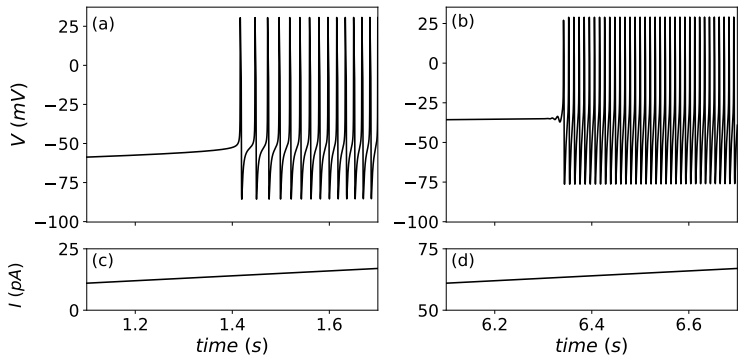

Figure 1.4: Example of neuronal response for class 1 (a) and class 2 (b) excitability to an external input that grows linearly in time I. Class 2 neurons need larger strength to perform sustained spikes. To perform the simulations we used the Morris-Lecar model, see Chapter 2 for details.

He identified three classes of responses, which lead to the Hodgkin classification:

> *Class 1 excitability:* The frequency of the action potentials can be very low and depends on the amplitude of the applied current. Indeed, we can observe the sequences of spikes in Fig. 1.4(a) where we simulated the response to the injection of a ramp current I into a neuron of class 1 (modeled with Morris-Lecar model, see Chapter 2 for details).
>
> *Class 2 excitability:* The frequency of the generated action potentials is limited to a certain band and the frequency is relative insensitive to the amplitude of the applied current. Simulated in Fig. 1.4 (b).
>
> *Class 3 excitability:* The neuron does not fire sustained spikes but single-spikes. Hodgkin named this class *sick* or *unhealthy*.

1.1.2 Neural noise

Noise is present in nerve cells, since neuronal activity has an intrinsic stochastic character: synapses may randomly release some neurotransmitters, ion channels can switch on and off arbitrarily, random input arriving from the activity of other neurons, intrinsic excitability of a neuron, etc. Noise influences the encoding and transmission of external signals or signals from other neurons, as well as the firing activity of single neurons.[12,13] Remarkably, noise in excitable systems can result in an oscillatory behavior: stochastic oscillations arise in excitable systems due to noise perturbations.[9] Yet, these noise-induced oscillations can have a most regular motion for

an optimal noise intensity; this phenomenon is known as *coherence resonance*.[14–22] In the same manner, noise can have a constructive role on the transmission of input signals in excitable systems: an optimal noise intensity enhances the detection of weak periodic or aperiodic signals; this phenomenon is known as *stochastic resonance*.[23–31] In particular, experiments on motor control in humans show that input noise provides a functional benefit in balance control. Specifically, weak mechanical noise applied to the feet can reduce significantly the postural sway in individuals.[32]

1.2 Neural coding

Sequences of action potentials are the language that the nervous system (and thus the central nervous system) uses to communicate. When we touch, the central nervous system decodes the sequences of spikes (or train of spikes) which thousands of sensory neurons emitted as a result of the change of pressure in our skin. When we hear, the central nervous system decodes the sequences of spikes which auditory neurons emitted as a result of the incoming pressure waves. Any kind of perception results in sequences of spikes (see Fig. 1.5 for an example) which the central nervous system processes.

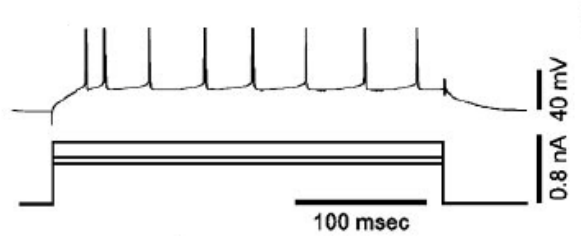

Figure 1.5: Train of spikes after a current injection in a cat cortical neuron. From.[33]

In turn, if there is the need of a response, the nervous system sends out other spike sequences to the motor neurons.[34] Although spikes are the information bits of the neural code,[35] there are other mechanisms than can play important roles in information processing. Sancristóbal and collaborators have shown that subthreshold oscillations influence the precise timing of action potentials.[36] Figure 1.6 shows the neuronal response to two synaptic inputs arriving at different times: either a spike is fired (blue solid line) or not, (red dashed line) depending on the phase of the subthreshold oscillation at the time when the synaptic input was received.[36]

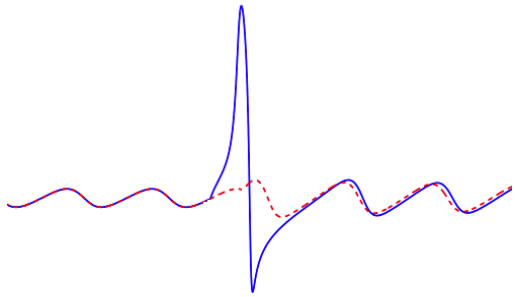

Figure 1.6: Schematic representation of subthreshold oscillations that influence the precise timing of action potentials: depending on their phase at the moment of the input, the neuron will fire or not. From.[36]

The other mechanism which has an important role in information transmission is bursting. A burst is composed by two or more spikes followed by a period of quiescence,[4] see Fig. 1.7. According to Krahe and Gabbiani[37] bursting can optimize the reliability of sensory information transmission across unreliable synapses.

This section focuses on how neurons encode and transmit inputs in the sequence of action potentials. Neurons can encode information of different types of signals using different

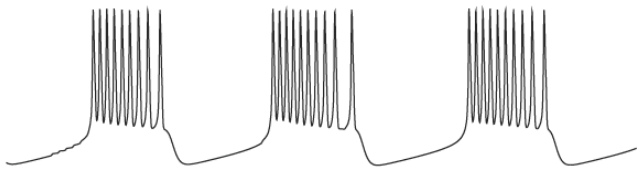

Figure 1.7: Schematic representation of bursting behavior. Neurons can fire either single spikes or bursts of spikes depending on the external perturbation and the intrinsic neuronal characteristics. From.[4]

encoding mechanisms. Next, we summarize some well-known mechanisms:

Single-cell coding

Single-cell coding states that the activity of single neurons is enough to encode and process information.[38] Back in the 1960s, Hubel and Wiesel[39–41] performed single-unit recordings in the visual cortex[b] of a cat which showed that single neurons were much more sensitive and selective to an external input than it was previously thought.[42] Jerry Lettvin[43] in 1969 coined the well-known term *grandmother cell*[44–48] to illustrate how neurons represented complex and specific concepts[c]. The grandmother cell would only respond to a highly specific, complex and meaningful stimulus such as the image of one's grandmother.[49] Although it is the term grandmother cell which exemplifies the concept of single-cell coding, some

[b] In mammals the brain is composed by the cerebrum, cerebellum and the brainsteam. The outer layer of the cerebrum is the cerebral cortex, where the visual cortex is located.[6]

[c] In 1969 Jerry Lettvin was a professor at the Massachusetts Institute of Technology. He had to give at short notice a course on biological foundations and wanted to illustrate how a neuron could represent a quite complex concept and came up with the idea of grandmother cells.[49]

years earlier to Lettvin's course, Konorski[50] already introduced a similar concept known as *gnostic neurons*. A gnostic neuron is a single neuron sensitive to complex stimuli such as faces, hands, emotions and animate objects. Gnostic neurons exemplify in a similar manner the concept of single-cell coding as the grandmother cells do. In 1992, Salzman and collaborators correlated the decision behavior and neuronal activity of a monkey when the monkey had to decide between random and coherent movement of a external stimulus. They showed that the external signal was encoded on the spike count produced by one neuron.[51] Also, Bialek and collaborators showed that individual spikes carried information about the time variation of a sensory stimulus.[34] Quiroga and collaborators reported that different pictures of celebrities, landmarks and objects selectively activated neurons of the human temporal lobe: a single neuron responded only to images of The Beatles; another neuron (from another patient) responded only to pictures of Jennifer Aniston, other neurons responded to images of Halle Berry, Julia Roberts and Kobe Bryant.[52]

Population coding

On the other hand, population coding states that the spikes fired by large population of neurons encode information. These neurons are broadly tuned, which means that they respond to a large variety of attributes of an stimulus, not only to one in particular.[53] Desimone and Gross reported face-selective cells which responded not only to a unique face but to other faces with similar sizes, orientations and colors.[54,55] Georgopoulos and collaborators analyzed an ensemble of 282 motor cortical

neurons of a subject while varying the direction of the subject's arm.[56] They found out that 80% of the neurons were broadly tuned: the activity of each neuron ranged over all arm's directions. Neuron activity was highest with movements in the preferred direction and lowest with movements on the opposite direction. This coding scheme is illustrated in Fig. 1.8, where the firing rate activity for three hypothetical neurons is plotted in function of the direction of movement. Each cell has a broad firing rate curve, yet if cell 1 and cell 2 are active, and cell 3 inactive, the direction of movement will be given by the overlapping region of cells 1 and 2, narrowing down the preferred direction of movement.[57]

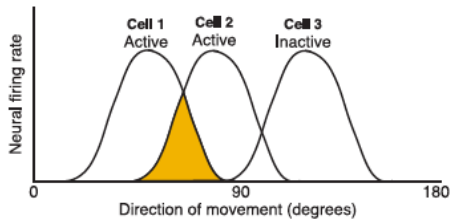

Figure 1.8: Scheme of population coding. From.[57]

Hybrid (or sparse) coding

While single-cell coding involves highly specialized neurons, population coding involves a large population of neurons broadly tuned. Instead, sparse coding involves a small number of neurons which respond to a specific and narrow range of attributes of the external stimuli.[44] For example, each cone photoreceptor is sharply tuned to light's location.[53] Another example of sparse coding comes from recordings of songbirds, where a sparse population of neurons underlies the generation of neu-

ral sequences. Each of those neurons only burst when a specific vocal element of the song is repeated.[58,59]

Cell assemblies coding
Cell assemblies are overlapping sets of neurons which code different information. An individual neuron can belong to different cell assemblies. The neurons are interconnected by flexible synapses, allowing for a dynamic reconstruction and deconstruction of the cell assembly.[38] Sakuray analyzed single neuronal activity from the rat hippocampal formation[d] and temporal cortex during the performance of auditory, visual, and auditory-visual tasks.[61] Of the total number of task-related neurons (i.e., neurons that showed activity during one of the tasks) almost 70% showed activity during more than one task, suggesting that each individual neuron is involved in more than one processing tasks.

Regardless of whether neurons use a single-cell code or a population code to encode information, they can encode information either in the number of spikes they fire (i.e., rate coding) or in the timing when the spikes are fired (i.e., temporal code).

Rate coding
In this coding scheme, the number of spikes a neuron fires in a given time window (known as firing rate) represents an attribute of the external stimulus. For a single neuron, the rate code is the firing rate; for a population of neurons, the rate code is the average of the individual firing rates. McAdams and Maunsell presented a bar of

[d]The hippocampal formation is a region in the temporal lobe of the brain that comprises the hippocampus and related structures. Memory, spatial navigation and control of attention take place in the hippocampal formation. It has a similar organization in all mammals.[60]

light to two subjects (two rhesus monkeys) and measured the firing rate of individual neurons from the visual cortex while varying the orientation of the bar of light. The firing rate of each neuron was higher or lower depending on the bar orientation, thus the firing rate encoded the orientation of the bar.[62]

Temporal coding

Temporal codes use the time of neural firing to encode the information about the stimulus.[63,64] For example, two different stimuli can elicit the same firing rate to a single neuron, however the evolution of the spike number over time for both stimuli can be different.[65] Richmond and collaborators recorded the activity of a cortex neuron of a monkey during the presentation of two different visual stimuli. The neuron elicited the same number of spikes over the whole counting interval, yet the number of spikes at each unit of time was not the same for both stimuli suggesting that precise timing encoded information about the stimulus. Mainen and Sejnowski[66] demonstrated that while neocortical rat neurons responded with imprecise spike trains to a flat stimulus, their response to weak input fluctuations was spike trains with precise time firing patterns. Berry and collaborators[63] measured retinal (tiger salamander and rabbit retina) responses to repeated visual stimuli. They demonstrated that the precise timing of a firing event carried several times more information than the spike count.

> Another example of a temporal code is present in songbirds: high vocal center (HVC)[e] neurons burst at the precise time a specific song syllabus takes place.[58]

Rate coding and temporal coding are the two major coding schemes in single cells and in populations of neurons, yet there are other coding mechanisms, which may be plausible in situations in which rate coding or temporal coding might not function.[68] Neural noise affects the encoding and transmission of information[13] and efforts have been focused on understanding its role in the neural code.[69–75]

As we will see in Chapter 3, for low neural noise rate coding encodes the period of an external weak signal applied to two coupled neurons, yet for intermediate and larger noise it does not: here we will propose another encoding mechanism (first proposed in[76]), which states that information can be encoded in the relative timing of the spikes (i.e., the sequence of time intervals between consecutive spikes: the sequence of interspike intervals).

1.3 Objectives and outline of the thesis

This thesis is devoted to the understanding of neural encoding and transmission of external, sub-threshold signals in the presence of noise. The starting point is the encoding mechanism Reinoso and collaborators presented in a recent work.[76] They showed that temporal patterns in the sequence of the interspike intervals of a neuron carry information about a weak external and periodic signal. By using this encoding mechanism,

[e] The HVC is a nucleus in the brain of songbirds which is in part responsible for acquisition and production of learned songs.[67]

the first objective of this thesis is to understand how a second neuron, which does not perceive the signal, affects the detection and the encoding of the signal, done by the first neuron. A second objective is to check the robustness of the encoding mechanism depending on (1) the class of neuron (class 1 or class 2), (2) the neuron model and on (3) the type of synapse (electrical and excitatory chemical) between two neurons. A third objective is to understand how the signal features (amplitude and frequency) are transmitted to the second neuron. The last objective is to investigate if this encoding mechanism is plausible also for neuronal ensembles.

The outline of the thesis is as follows. Chapter 2 presents the models used to simulate neuronal spike sequences and the methods used to analyze them. In Chapter 3 we show that the encoding mechanism proposed in[76] is robust to the coupling of a second neuron. In Chapter 4 we analyze how the encoding mechanism is affected by the class of neuron and the type of synapse. In Chapter 5 we analyze the activity of a group of neurons, when they all perceive a weak periodic signal. We show that neuronal coupling is beneficial for signal encoding as a group of neurons is able to encode a small-amplitude signal, which could not be encoded when it is perceived by just one or two coupled neurons. Finally, Chapter 6.2 presents our conclusions and discusses future research.

Chapter 2

Models and methods

2.1 Models

The biophysical mechanisms responsible for neural activity provide a basis for the design of neuronal models. Neuronal models can either give detailed descriptions of these mechanisms (such as the generation and propagation of action potentials, or the time-evolution of membrane currents) by involving several differential equations. Or they can just focus on the mathematical properties of neural excitation by just involving one or two differential equations.[8] Back in 1952 Hodgkin and Huxley[77] studied the flow of electric current through the surface membrane of a giant squid nerve fiber and succeeded to model the dependencies of the membrane potential with the membrane currents and vice versa.[4] Hodgkin and Huxley jointly received the 1963 Nobel Prize in Physiology or Medicine *for their discoveries concerning the ionic mechanisms involved in excitation and inhibition in the peripheral and central portions of the nerve cell membrane.* The Hodgkin-Huxley model is now an important model in computational neuroscience, it is a four-dimensional dynamical system, which describes membrane potential, activation and inactivation of sodium current and activation of potassium current[78] (equations are not included here, for a detailed description see[8,78]). Figure 2.1(a) reproduces the original numerical solution given by Hodgkin

and Huxley[77] and Fig. 2.1(b) depicts the trace of a recorded action potential of the giant squid axon.

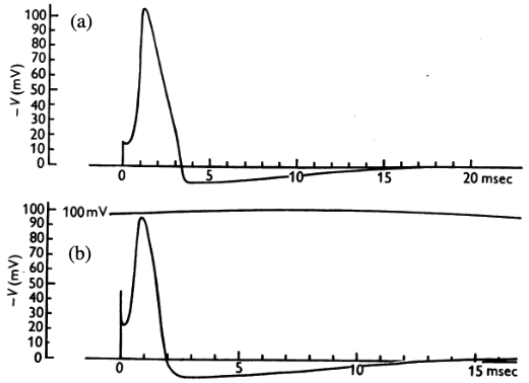

Figure 2.1: (a) Numerical solution for the Hodgkin-Huxley equations for initial depolarization at 15 mV. (b) Trace of a recorded action potential. From.[77]

The Hodgkin-Huxley model can exhibit (under parameter tuning) the most prominent features of biological spiking neurons (such as tonic spiking and bursting). It is a conductance-base model which allows to study the dependence of the neuronal behavior on measurable physiological parameters (such as maximal conductances) but it is computationally expensive to implement. Richard FitzHugh analyzed the Hodgkin-Huxley model and demonstrated that one can capture mathematically the properties of excitation and propagation of the sodium and potassium currents with only two dimensionless differential equations which do not have neither conductances nor currents dependencies.[79] Nagumo and collaborators electronically simulated the proposed equations using tunnel diodes,[80] since tunnel diodes have a current-voltage curve similar to the cubic shape FitzHugh implemented. From then on these equations are named as the FitzHugh-Nagumo (FHN) equations.[81] On the other hand, Cathy Morris and

Harold Lecar studied the excitability of a giant muscle fiber of a huge barnacle and presented a conductance-based model (all the different parameters in the equations are experimentally measurable) but only two-dimensional.[82] This model is a simplification of the conductance processes in the barnacle, but allows to correctly mimic the different oscillation phenomena that Morris and Lecar observed experimentally: they could model the three main classes of neuron excitability (see Section 1.1 for details) by changing model parameters.[83] Since these early studies, many models have been proposed in the literature, which have either higher or lower degree of complexity.[78] In this thesis we use these two models (FitzHugh-Nagumo and Morris-Lecar) because they offer a good compromise between realistic spike-generation modeling and computational cost.

2.1.1 FitzHugh-Nagumo model

One common representation of a single and deterministic FitzHugh-Nagumo oscillator is as follows[a]:

$$\epsilon \dot{u} = u - \frac{u^3}{3} - v, \tag{2.1}$$

$$\dot{v} = u + a.$$

The model consist of two dimensionless variables, named *voltage-like variable* u, or excitation variable, which is responsible for the upstroke of the spike. It mimics the depolarization of the neuron, and the *recovery variable* v, which is responsible for the downstroke of the spike. It mimics the repolarization of the neuron. Mathematically, it provides a negative feedback to the voltage-like variable.

[a] The general form of the FitzHugh-Nagumo includes a linear v-dependence in the second equation.[81]

When modeling the neuronal dynamics, variables u and v need to have different time-scales: in order to perform a spike the increment of u has to be faster than the increment of v, thus the parameter ϵ it is usually $\epsilon \ll 1$. For this reason, usually u is known as the fast variable whereas v is called the slower variable. In this thesis we use the value $\epsilon = 0.01$, which has been frequently used in the literature.[9,17,22] The parameter a is the so called bifurcation parameter[b]. The FitzHugh-Nagumo system undergoes a supercritical Hopf bifurcation at $a = 1$: it changes from a stable fixed point (for $a > 1$ it displays no activity) into an unstable one (for $a < 1$ the system displays self-sustained regular oscillations).[84] Figure 2.2 shows the evolution of the voltage-like variable while increasing the bifurcation parameter a. In the excitable regime, the system resides on the rest state, yet if a strong enough perturbation happens, the system leaves the stable state and goes through the firing and the following refractory state, performing a spike.[9]

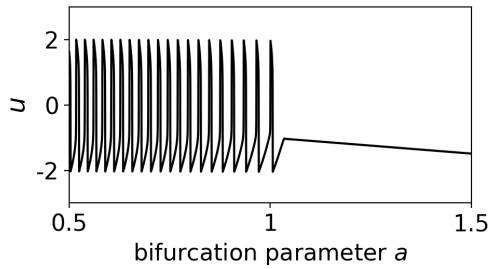

Figure 2.2: Voltage-like variable u as a function of the bifurcation parameter a for $\epsilon = 0.01$. At $a = 1$ the system undergoes the Hopf bifurcation.

[b]Bifurcations are qualitative changes in the dynamics of a system, the parameter values at which they occur are named *bifurcation parameters*.[84]

In this thesis we will consider excitable, stochastic and coupled FitzHugh-Nagumo oscillators. The FitzHugh-Nagumo model has been extensively used to investigate the phenomena of stochastic resonance and coherence resonance[17,22–25,27–31,85,86] (see subsection 1.1.2). It has also been widely employed to model neuronal ensembles[87] and other excitable systems such as cardiac cells.[88–93]

2.1.2 Morris-Lecar model

In this thesis we also consider the Morris-Lecar model:[4,94]

$$\begin{aligned} C\dot{V} =& m_\infty(V)\cdot g_f\cdot(E_{\mathrm{Na}}-V)+ \\ &+W\cdot g_s\cdot(E_{\mathrm{k}}-V)+g_l\cdot(E_{\mathrm{l}}-V)+g_{po}, \end{aligned} \tag{2.2}$$

$$\dot{W}=\phi_W\frac{W_\infty(V)-W}{\tau_W(V)}, \tag{2.3}$$

$$m_\infty(V)=0.5\left[1+\tanh\left(\frac{V-\beta_m}{\gamma_m}\right)\right], \tag{2.4}$$

$$w_\infty(V)=0.5\left[1+\tanh\left(\frac{V-\beta_w}{\gamma_W}\right)\right], \tag{2.5}$$

$$\tau_w(V)=\frac{1}{\cosh\left(\frac{V-\beta_w}{2\gamma_W}\right)}. \tag{2.6}$$

where V is the fast activation variable and W is the slower recovery variable. The parameters E_{k}, E_{Na} and E_{leak} represent the equilibrium potentials of Na^+ (fast), K^+ (slow) and of leak currents; g_f, g_s and g_l denote the maximal conductances for Na^+, K^+ and leak currents, respectively. The main parameters of the model are (the same as those used in[94]): $E_{Na}=50$ mV, $E_K=-100$ mV, $E_l=-70$ mV, $g_f=20\mathrm{mS/cm}^2$, $g_s=20$

mS/cm^2, $g_l = 2$ mS/cm^2, $\phi_W = 0.15$, $C = 2$ μF/cm^2, $\gamma_m = 18$ mV, $\beta_W = -10$ mV and $\gamma_W = 13$ mV. Varying β_m allows to change from class 1 to class 2 (see subsection 1.1.1): for class 1, beta=-12; for class 2, beta=0. The synaptic conductance g_{po} regulates the intensity of an external source of noise, which follows a Poisson distribution with rate R and it is responsible for the spiking of the neurons. It mimics n-excitatory pre-synaptic neurons, not included in the model, with a spiking rate of R/n.

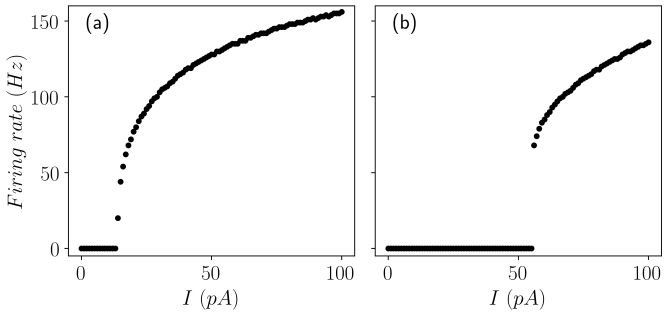

Figure 2.3: Current-frequency curve for (a) class 1 ($\beta_m = -12$ mV) and (b) class 2 ($\beta_m = 0$ mV).

Qualitatively, the distinction between class 1 and class 2 neurons is given by the response to an external current. The frequency of class 1 neurons increases continuously while increasing an external current; whereas for class 2 neurons, the frequency increases discontinuously, as we can see in Fig. 2.3. For each class of excitability the Morris-Lecar model undergoes a different type of bifurcation. For class 1 excitability the system performs a saddle-node on invariant cycle (SINC) bifurcation (the system's fixed point is destroyed), whereas for class 2 the system performs a subcritical Hopf bifurcation (system's fixed point is destabilized); yet for both bifurcations the neurons changes from remaining at a stable and sub-threshold

voltage to regular firing.[94] Table 2.1 summarizes the parameters used for each class.

Parameters	Class 1	Class 2
$E_{Na}(mV)$	50	50
$E_K(mV)$	-100	-100
$E_{leak}(mV)$	-70	-70
$g_{fast}(mS/cm^2)$	20	20
$g_{slow}(mS/cm^2)$	20	20
$g_{leak}(mS/cm^2)$	2	2
$C(\mu F/cm^2)$	2	2
$\phi_w(mS/cm^2)$	0.15	0.15
$\beta_w(mV)$	-10	-10
$\gamma_w(mV)$	13	13
$\gamma_m(mV)$	18	18
$\beta_m(mV)$	-12	0

Table 2.1: Parameters of the Morris-Lecar model used for the simulation of class 1 and 2 neurons.

2.1.3 Model simulations and spike detection

For the FitzHugh-Nagumo model we used the simplest numerical method for solving an stochastic rate equation (also known as Euler-Maruyama method[95]), with an integration step of $dt = 10^{-3}$. The integration was computed until 10^5 spikes were generated for each set of parameters. The temporal interval between two subsequent spikes is $\mathrm{ISI}_i = T_{i+1} - T_i$ with T_i defined with the condition $u(T_i) = 0$ (considering just the ascensions).

For the Morris-Lecar model we used the numerical method Runge-Kuta of order 4 with an integration step of $dt = 0.01$ ms. The integration was computed until 15000 spikes were

generated for each set of parameters. Here, T_i was defined with the condition $V(T_i) = 20$ mV.

2.2 Time-series analysis of spike sequences

2.2.1 Spike regularity

The regularity of the inter-spike interval (ISI) sequence is characterized by the coefficient R,[17] also known as coefficient of variation (Cv), which has been extensively used to detect both stochastic resonance and coherence resonance:

$$R = \frac{\sqrt{\langle \mathrm{ISI}^2 \rangle - \langle \mathrm{ISI} \rangle^2}}{\langle \mathrm{ISI} \rangle}, \tag{2.7}$$

where $\langle \mathrm{ISI} \rangle$ and $\langle \mathrm{ISI}^2 \rangle$ are the mean and the variance of the sequence of inter-spike intervals: $\{\mathrm{ISI}_1, ..., \mathrm{ISI}_i, ..., \mathrm{ISI}_N\}$ where $\mathrm{ISI}_i = T_{i+1} - T_i$ with T_i and T_{i+1} being the times when two consecutive spikes occur.

Linear correlations between ISIs are quantified by the serial correlation coefficients (SCCs):

$$\mathrm{C}_j = \frac{\langle (\mathrm{ISI}_i - \langle \mathrm{ISI} \rangle)(\mathrm{ISI}_{i-j} - \langle \mathrm{ISI} \rangle) \rangle}{\langle \mathrm{ISI}^2 \rangle - \langle \mathrm{ISI} \rangle^2} \tag{2.8}$$

where j is an integer number. The serial correlation coefficient C_j measures if ISI_i and ISI_{i+j} are correlated (i.e., if ISI_i influences the value of ISI_{i+j}). For example, for $j = 1$ a negative value of C_1 indicates that a short ISIs tends to be followed by a short one and vice versa (if ISI_i is larger than the average, it implies that ISI_{i+1} will tend to be smaller than the average and

vice versa). On the other hand, if $C_j = 0$, it implies that any given ISI for all $j \neq 0$ is independent of the previous ISIs.[73] A drawback of the SCCs is that they only detect linear relations and therefore, nonlinear analysis tools are needed in order to detect nonlinear correlations.

2.2.2 Ordinal analysis

Ordinal analysis[96] is a symbolic methodology which has been demonstrated to be well suited for detecting nonlinear correlations in spike trains.[76,97,98] In this approach the actual ISI values $\{\mathrm{ISI}_1, ..., \mathrm{ISI}_i, ..., \mathrm{ISI}_N\}$ are not taken into account, instead, their relative temporal ordering is considered. Ordinal analysis transforms a time series into a sequence of symbols, which are known as ordinal patterns. Here, ordinal analysis is used to study the spike trains of neurons and the ordinal patterns are defined by the relative order of L consecutive ISI values. We will apply ordinal analysis to the sequence of ISI values $\{\mathrm{ISI}_1, ..., \mathrm{ISI}_i, ..., \mathrm{ISI}_N\}$. For each interval ISI_i the subsequent $L - 1$ intervals are considered and compared. The total number of possible order relations (i.e., ordinal patterns of length L) is equal to the number of permutations $L!$. If we set $L = 2$ we have only two patterns: 12 and 21 for $\mathrm{ISI}_1 < \mathrm{ISI}_2$ and $\mathrm{ISI}_1 > \mathrm{ISI}_2$, respectively; if we set $L = 3$, we have $3! = 6$ possible ordinal patterns, which are listed in Table 2.2.

For example, if we consider the following sequence of intervals $\{4.9, 3.4, 3.3, 3.2, 5.0, ...\}$. The first value $\mathrm{ISI}_1 = 4.9 > \mathrm{ISI}_2 = 3.4 > \mathrm{ISI}_3 = 3.3$ and consequently the ordinal pattern is 210. In the next pattern $\mathrm{ISI}_2 > \mathrm{ISI}_3 > \mathrm{ISI}_4$ and the ordinal pattern 210 repeats. But when starting with ISI_3 we get the pattern 102 because $\mathrm{ISI}_3 > \mathrm{ISI}_4$ but $\mathrm{ISI}_5 > \mathrm{ISI}_3$.

When comparing two ISIs which are equal, a small random noise is added in one of them.

In this thesis we have used $L = 3$, which allows to investigate the order relation among 3 inter-spike intervals, i.e., four consecutive spikes. This choice is motivated by the fact that we focus on sub-threshold signals and the neuron's firing activity is driven by noise (without noise, there are no spikes). Therefore, ISI correlations among consecutive spikes are expected to be short range. In addition, as the number of possible patterns increases as L!, we would need to perform much longer simulations in order to obtain longer ISI sequences that would the reliable detection of longer correlations.

Symbol	Relation
012	$\mathrm{ISI}_3 > \mathrm{ISI}_2 > \mathrm{ISI}_1$
021	$\mathrm{ISI}_2 > \mathrm{ISI}_3 > \mathrm{ISI}_1$
102	$\mathrm{ISI}_3 > \mathrm{ISI}_1 > \mathrm{ISI}_2$
120	$\mathrm{ISI}_2 > \mathrm{ISI}_1 > \mathrm{ISI}_3$
201	$\mathrm{ISI}_1 > \mathrm{ISI}_3 > \mathrm{ISI}_2$
210	$\mathrm{ISI}_1 > \mathrm{ISI}_2 > \mathrm{ISI}_3$

Table 2.2: Ordinal patterns for $L = 3$.

The symbolic sequence of ordinal patterns is computed using the function `perm_indices` defined in.[99] Then, the ordinal probabilities are estimated as $p_i = n_i/M$ where n_i denotes the number of times the i-th pattern occurs in the sequence, and $M = N - (L - 1)$ denotes the total number of patterns (N is the length of the ISI sequence). If the patterns are equiprobable one can infer that there are no preferred order relations in the timing of the spikes. On the other hand, the presence of frequent (or infrequent) patterns will result into a non-uniform distribution of the ordinal patterns. A binomial test will be

used to analyze the significance of preferred and infrequent patterns: if all the ordinal probabilities are within the interval $[p - 3\sigma_p, p + 3\sigma_p]$ (with $p = 1/L!$ and $\sigma_p = \sqrt{p(1-p)/M}$), the probabilities are consistent with the uniform distribution (with 99.74% confidence level) else, if at least one probability value lies outside the interval, there are significant deviations which reveal the presence of over expressed and/or less expressed patterns. In order to quantify at once these deviations we compute the *permutation entropy* H,[96] defined as

$$H = \frac{-\sum_i p_i \log p_i}{\log L!}. \tag{2.9}$$

We normalize H to its maximum value $H_{max} = \log L!$. H ranges between 0 (regular and deterministic behavior) and 1 (completely noisy and random behavior). Already small deviations from $H = 1$ can be used to identify deviations from a fully noisy behavior. As explained before, because we consider parameters such that the signal and the coupling terms are subthreshold and the spikes are noise-induced, a large number of spikes are needed to precisely estimate the ordinal probabilities (see Fig. 2.4, reproduced from[76]). In this thesis the total number of spikes is set to 15000 (chapter 4) and 10^5 (chapter 3 and chapter 5).

Time-series of ordinal patterns

Given a sequence of $N + 1$ spikes that occur at times $\{T_1, ..., T_{N+1}\}$, the sequence of inter-spikes intervals is $\{\mathrm{ISI}_1, ..., \mathrm{ISI}_i, ..., \mathrm{ISI}_N\}$. As stated before we can transform it into a sequence of $M = N - (L - 1)$ ordinal patterns and analyze the frequency of occurrence of the different patterns.

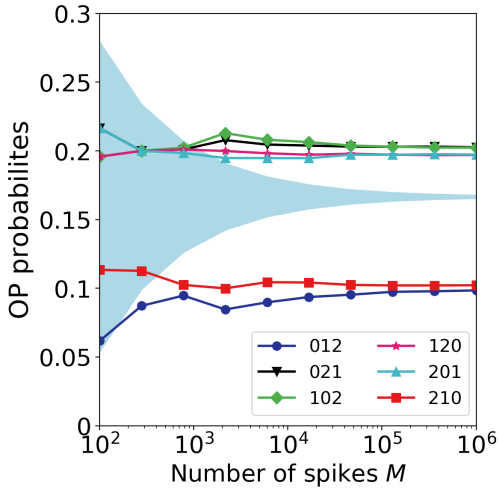

Figure 2.4: Probabilities of the six ordinal patterns in function of the number of spikes M for the single and stochastic FitzHugh-Nagumo neuron coupled to a weak external signal. We used Eq. 3.1 with the parameters $\sigma = 0$, $a_0 = 0.05$, $D = 10^{-5}$, and $T = 10$. Figure reproduced from.[76]

However, these probabilities do not provide information about the time evolution of the ordinal patterns.

Here, we introduce the time-series of the ordinal patterns $s(t)$, which keeps track of the ordinal patterns at each time step. Setting $L = 3$, $s(t) \in \{012, 021, 102, 120, 201, 210\}$. The temporal order among the first three inter-spike intervals (i.e., four spikes) $\{\mathrm{ISI}_1, \mathrm{ISI}_2, \mathrm{ISI}_3\}$ defines the first ordinal pattern s_1 and the time of occurrence of the 4th spike sets the initial time t_0 of the time-series. The first ordinal pattern s_1 will be kept along time until a new spike will occur at time t_i, then the second ordinal pattern s_2 will be defined at time t_i with the sequence $\{\mathrm{ISI}_2, \mathrm{ISI}_3, \mathrm{ISI}_4\}$. We will apply this procedure for the $M - 1$ ordinal patterns. The time step between the spiking times T_i and T_{i+1} and the number of ordinal patterns

M determines the length of the time-series. In Fig. 2.5 we have an example of the correspondent $s_1(t)$ for a given $u_1(t)$ (where subscript 1 refers to neuron index).

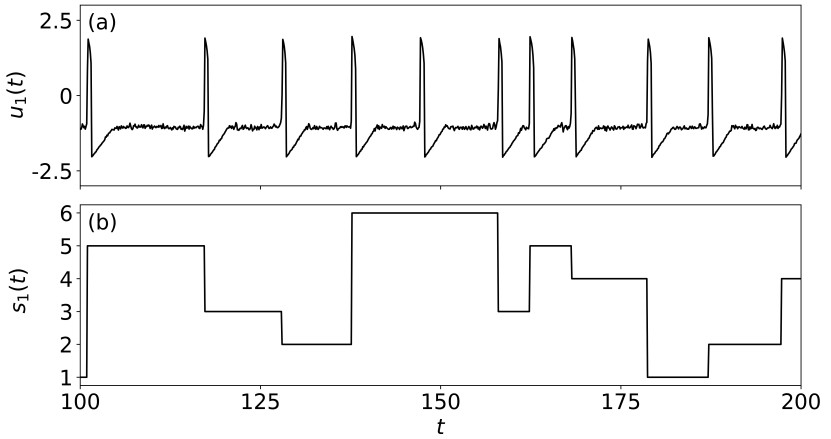

Figure 2.5: (a) Time-series of the voltage-like variable $u_1(t)$ and (b) the correspondent ordinal time-series $s_1(t)$ for neuron 1. The parameters are $a_0 = 0.05$, $D = 2.5 \cdot 10 \cdot 10^{-5}$, $\sigma = 0.05$ and $T = 10$. See Eqs. 3.1 for parameter definition.

In this thesis, we will use the time-series of ordinal patterns to compute the mutual information between two time-series; which it can be regarded as a synchronization measure.

2.2.3 Synchronization measures

Cross-correlation function

The cross-correlation function between two discrete variables is a linear measure of synchronization. We will apply it to the time-series of the voltage-like variable of neuron 1 $\{u_{1_1}, ..., u_{1_N}\}$

and to the time-series of the voltage-like variable of neuron 2 $\{u_{2_1}, ..., u_{2_N}\}$. The cross-correlation function is defined as

$$c_{u_1 u_2} = \frac{\langle (u_i - \langle u \rangle)(u_{i-j} - \langle u \rangle) \rangle}{\langle u^2 \rangle - \langle u \rangle^2} \tag{2.10}$$

where $\langle u_1 \rangle$ and $\langle u_2 \rangle$, are the mean of the voltage-like variable of neuron 1 and neuron 2, respectively. The absolute value of the cross-correlation function ranges from zero (u_1 and u_2 are asynchronous) to one (complete synchronization).

Mutual information

Synchronization can be also measured with information theory concepts. The mutual information of two random variables X and Y indicates the amount of information shared by X and Y.[100] We will use this concept to measure the amount of information shared by the spike trains of two neurons, using the time-series of ordinal patterns, previously introduced.

The mutual information I is

$$I = H_1 + H_2 - H_{1,2} \tag{2.11}$$

where H_1 and H_2 are the entropies computed from the time-series of the ordinal patterns and $H_{1,2}$ is the join permutation entropy, defined as

$$H_{1,2} = -\frac{\sum_i \sum_j p_{ij}^{12} \log p_{ij}^{12}}{\log L!}, \tag{2.12}$$

where p_{ij}^{12} is the probability that the i-th pattern in neuron 1 occurred at the same time as the j-th pattern in neuron 2, and M is the length of the ordinal pattern time-series.

If the time-series of ordinal patterns are independent from each other $H_{1,2} = H_1 + H_2$, and thus $I = 0$ (in the limit of a very long time series), which is the minimum value the mutual information can take. On the other hand, if both time-series are equal, the mutual information reaches its maximum value at $I = H_1 = H_2$. We can regard the mutual information as a synchronization measure, since it quantifies the information we can gain about one variable from the other. The more information we obtain, the more synchronized they are. Since the mutual information computed from finite time series returns a positive number, it is necessary to analyze if the obtained result is statistically significant. This can be done by using surrogate data.[101]

Chapter 3

Signal encoding and transmission by two FitzHugh-Nagumo neurons

In this chapter we consider two FitzHugh-Nagumo neurons[79,80] (see Sec. 1.3), mutually coupled (as indicated in Fig. 3.1), with a weak periodic signal applied to one of them (referred to as neuron 1). We study how neuron 1 encodes the weak signal and how it is transmited to neuron 2 (how the spikes fired by neuron 2 contain the signal information). The results of the analysis of signal encoding were published in.[102] The model equations are:

$$\begin{aligned}
\epsilon_1 \dot{u_1} &= u_1 - \frac{u_1^3}{3} - v_1 + a_0 \cos(2\pi t/T) + \sigma_1 u_2 + \sqrt{2D}\xi_1(t), \\
\dot{v_1} &= u_1 + a_1, \\
\epsilon_2 \dot{u_2} &= u_2 - \frac{u_2^3}{3} - v_2 + \sigma_2 u_1 + \sqrt{2D}\xi_2(t) \\
\dot{v_2} &= u_2 + a_2
\end{aligned} \tag{3.1}$$

where u_i and v_i are a voltage-like and a recovery-like variables, for neuron i. The coupling is assumed to be linear and instantaneous and it is characterized by the coupling strength

σ. The weak periodic signal has amplitude a_0 and period T. The external perturbation is modeled as Gaussian white noise, with amplitude D. White noise forces $\xi_i(t)$ and $\xi_i(t')$ for $t \neq t'$ are statistically independent, thus $\langle \xi_i(t)\xi_i(t') \rangle = \delta(t - t')$. As well, Gaussian white noise fullfills that $\langle \xi_i(t) \rangle = 0$. Here we have to consider the coupling term σ for which the intrinsic dynamics of the system changes. With coupling the supercritical Hopf bifurcation will take place at $a^2 = 1 + \sigma$, thus for $a^2 > 1 + \sigma$ the system be on the excitable regime. Therefore, the bifurcation parameter is set to $a = 1.05$ and coupling strength is within the interval $\sigma \in [0, 0.1]$. The modulation amplitude and period are varied such that the input signal is kept subthreshold (without noise there are no spikes but only subthreshold oscillations).

The main part of the chapter focuses on two identical neurons, i.e., $\epsilon_1 = \epsilon_2 = \epsilon$ and $a_1 = a_2 = a$. Thus, unless otherwise stated, $\epsilon = 0.01$ and $a = 1.05$. In Section 3.4.1 we analyze two coupled non-identical neurons.

As explained before, the model equations are simulated, from random initial conditions, using the Euler-Maruyama method with an integration step of $dt = 10^{-3}$. For each set of parameters, the voltage-like variable of each neuron u_i is analyzed and the sequence of inter-spike-intervals (ISIs) is computed, $\{\mathrm{ISI}_{j_i}; \mathrm{ISI}_{j_i} = (t_{j+1} - t_j)_i\}$ with t_j defined by the condition $u_i(t_j) = 0$, considering only the ascensions.

Figure 3.2 displays the voltage-like variable of neuron 1, u_1, in different situations. When there is no noise, no signal and no coupling, the neuron is in the rest state and when the subthreshold signal is applied, u_1 displays small sub-threshold oscillations [panel (a)]; when noise is added, noise-induced spikes are observed, which carry information about the applied sub-

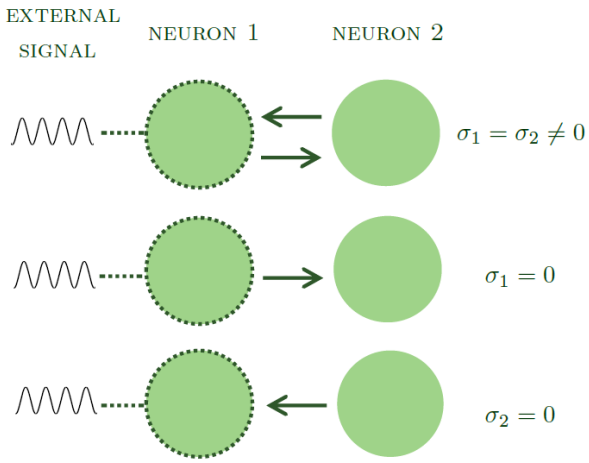

Figure 3.1: Schematic representation of two mutually coupled neurons, one of which (neuron 1) perceives a periodic input signal. σ_1 and σ_2 represent the strength of the coupling of neuron 2 to neuron 1, and of neuron 1 to neuron 2, respectively.

threshold signal [panel (b)]; and when the coupling to neuron 2 is added, a noticeable effect is the increase of the firing rate [panel (c)]. The differences that are qualitatively observed in these time series are going to be quantitatively addressed by using the methods of analysis presented in Chapter 2.

3.1 Sub-threshold region in the parameter space (a_o, T)

We first have to distinguish between a sub-threshold and a super-threshold signal, as we are interested in the encoding of weak signals. The first one refers to a signal which, in the absence of noise, it does not induce any spike [u_1 displays small oscillations, as in Fig. 3.2(a)], while the second one is a signal that is strong enough to induce spikes. A periodic signal

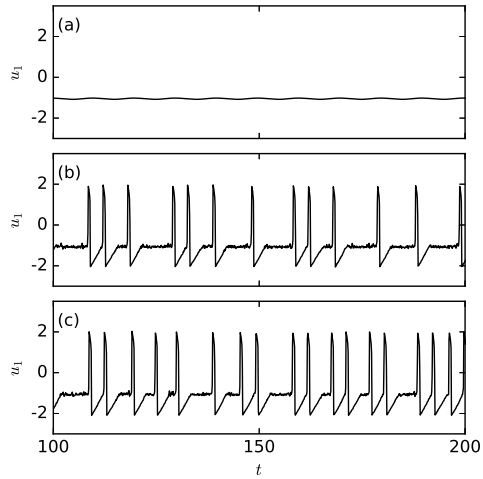

Figure 3.2: Time series of the voltage-like variable of neuron 1 when (a) the signal is applied, and there is no noise and no coupling; (b) the signal is applied and there is noise but no coupling and (c) the signal is applied and there is noise and coupling. The parameters are $a_0 = 0.05$, $T = 10$ and (a) $D = 0$, $\sigma_2 = 0$; (b) $D = 2 \cdot 10^{-6}$, $\sigma = 0$; (c) $D = 2 \cdot 10^{-6}$, $\sigma = 0.05$.

can be either sub-threshold or super-threshold depending on both, the period and the amplitude. Thus, to identify the parameters where the signal is sub-threshold, in Fig. 3.3 we plot in color code the spike rate (i.e., the inverse of the mean ISI, $1/\langle \text{ISI} \rangle$), as a function of a_0 and T for both situations $D = 0$ and $D \neq 0$. In panel (a) neuron 1 is isolated ($\sigma_2 = 0$), while in panel (b) it is coupled to neuron 2 ($\sigma_1 = \sigma_2 = 0.05$) and for both panels $D = 0$.

For no noise, when the neuron is uncoupled, for large amplitude and/or small period the signal is super-threshold, otherwise is sub-threshold. When the neuron is coupled to neuron 2, we note that the super-threshold region is slightly larger in the parameter space (a_0, T), as compared to the uncoupled case.

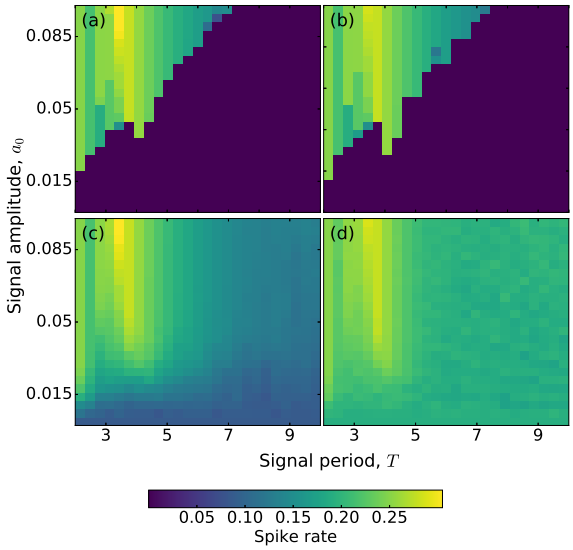

Figure 3.3: Influence of the signal parameters in the spike rate. The spike rate of neuron 1 in color code is plotted as a function of the signal amplitude, a_0, and period, T. Panels (a) and (b) display the deterministic spike rate ($D = 0$) without coupling ($\sigma_1 = \sigma_2 = 0$) and with coupling ($\sigma_1 = \sigma_2 = 0.05$), respectively. In panels (c) and (d) the noise is included ($D = 2 \cdot 10^{-6}$).

When we include noise, Figs. 3.3(c) and (d), we first note that in the super-threshold region (yellow) the spike rate does not change significantly (it is about the same as for D=0). This is due to the fact that in this region the spikes are mainly induced by the signal. In contrast, in the sub-threshold region, comparing the uncoupled (panel c) and the coupled (panel d) situations, we note that coupling significantly increases the spike rate (it almost doubles). Therefore, in this region coupling plays the role of an extra source of noise.

3.2 Influence of coupling coefficients on the spike rate

Having identified the sub-threshold region in the parameter space (a_0, T), we next turn our attention to the influence of the coupling coefficients. Figure 3.4 displays the spike rate as a function of σ_1 and σ_2 in different situations. In panel (a) there is no signal and no noise. We observe that when both $|\sigma_1|$ and $|\sigma_2|$ are large enough, the coupling induces spikes. Positive coupling coefficients result in a higher spike rate, in comparison with negative coefficients. In panel (b), the noise is still zero but a weak signal is applied. Because the signal is subthreshold [$a_0 = 0.05$ and $T = 10$, which are in the sub-threshold region in Figs. 3.3(a),(b)], we note only small variations with respect to panel (a).

In Figures 3.4 (c) and (d) noise is included; in (c) there is no signal while in (d) the weak signal is applied. To show how the spike rate changes with the coupling, Figs. 3.4 (c) and (d) display the relative variation of the spike rate (with respect to the spike rate when neuron 1 is uncoupled). Without signal (panel c), positive coupling coefficients result in larger spike rate as compared to negative ones, however, when the signal is applied (panel d) these differences are washed out. The vertical line in panels (c) and (d) is due to the fact that when $\sigma_1 = 0$ neuron 1 is uncoupled from neuron 2, and thus its spike rate does not depend of σ_2.

In order to limit the number of parameters, in the following we assume $\sigma_1 = \sigma_2 = \sigma$ and fix (unless otherwise stated) $\sigma = 0.05$, $a_0 = 0.05$ and $T = 10$. For these parameters the signal and the coupling act as sub-threshold perturbations: without noise neuron 1 does not fire spikes.

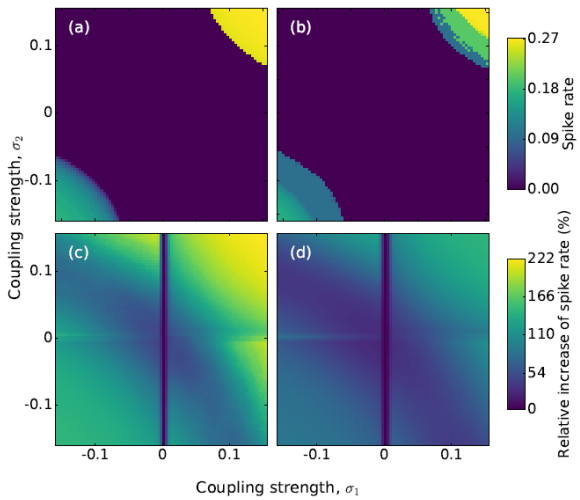

Figure 3.4: Influence of the coupling strengths in the spike rate. In (a) and (b) the deterministic ($D = 0$) spike rate of neuron 1 is plotted in color code, as a function of σ_1 and σ_2, when the signal is not applied ($a_0 = 0$) and when it is applied ($a_0 = 0.05$ and $T = 10$), respectively. Panels (c) and (d) display the relative increase of the spike rate (with respect to the uncoupled neuron), when noise is included ($D = 2 \cdot 10^{-6}$). In (c) $a_0 = 0$ while in (d), $a_0 = 0.05$ and $T = 10$.

3.3 Influence of noise and modulation parameters on the spike rate

To further characterize the role of noise, Fig. 3.5 displays the mean ISI, $\langle \text{ISI} \rangle$, as a function of noise intensity for different periods of the applied signal. In panel (a) $\sigma = 0$, while in panel (b), $\sigma = 0.05$. For both cases there is clearly a noise dominated regime, where $\langle \text{ISI} \rangle$ is the same, regardless of the coupling and of the period of the signal. In contrast, for low noise levels the coupling and the period affect the $\langle \text{ISI} \rangle$. In panel 3.5 (a) ($\sigma = 0$) we can also compare the mean ISI when the signal is applied (solid symbols indicate $a_0 \neq 0$ and different periods)

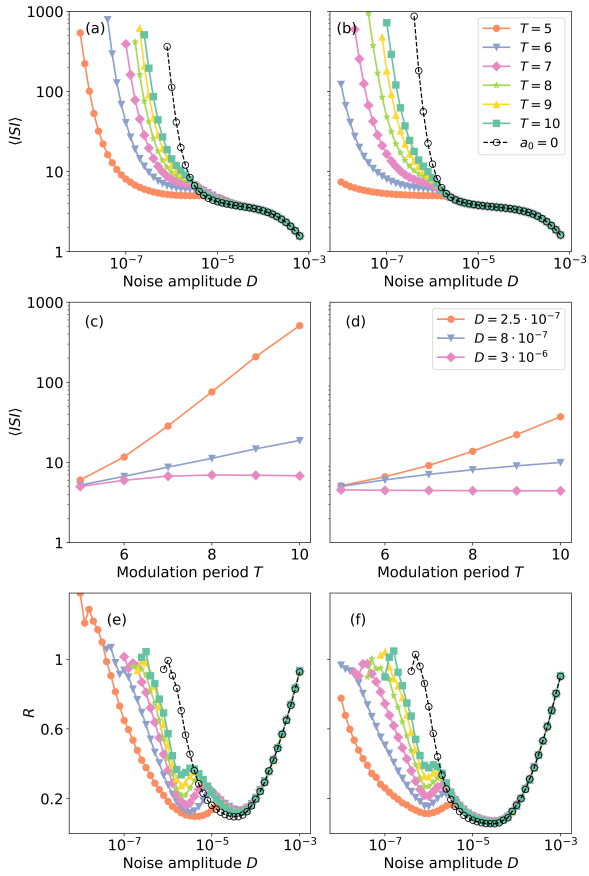

Figure 3.5: Influence of the noise strength in the mean ISI and in the regularity of the spikes. (a), (b) Mean ISI, $\langle \text{ISI} \rangle$, of neuron 1 as a function of the noise strength, D, for different periods, T, of the signal; (c), (d) $\langle \text{ISI} \rangle$ vs. T and (e), (f) ISI normalized standard deviation, R, as a function of D. Panels (a), (c) and (e) are without coupling ($\sigma = 0$), while (b), (d) and (f) are with coupling ($\sigma = 0.05$).

and when the signal is not applied (empty circles): we see that, when $a_0 \neq 0$ the neuron fires at lower noise intensities as compared to $a_0 = 0$. Comparing panel 3.5 (a) with panel 3.5 (b) ($\sigma = 0.05$) we note that when neuron 1 is coupled to neuron 2, it starts firing at even lower noise intensities.

Regarding the role of the period of signal, when the noise level is low, the larger T is, the larger $\langle \mathrm{ISI} \rangle$ is. There is a linear relation, as shown in Figs. 3.5(c) and (d), which holds for both, the coupled and the uncoupled cases. For stronger noise, $\langle \mathrm{ISI} \rangle$ remains constant when increasing T.

Noise-induced regularity in the spike train[17,103,104] is characterized in panels (e) and (f), where the normalized standard deviation of the ISI distribution, R, is plotted against the noise intensity for different T, without and with coupling, respectively. In both panels, two minimums are observed. Whereas the first one indicates stochastic resonance,[105–107] as it occurs when $T \sim \langle \mathrm{ISI} \rangle$, the second one reveals the coherence resonance phenomenon,[17,108] which is independent from the period of the signal. It occurs for an intermediate value of the noise amplitude for which noise-induced oscillations become most coherent. For some periods T a maximum appears for very small values of the intensity of the noise. Such maxima are a signature of anticoherence resonance.[109]

Next, we discuss how the shape of the ISI distribution depends on the amplitude and on the period of the signal, and how it is affected by the coupling.

Figure 3.6 and Fig. 3.7 display the ISI distribution for different values of the period and of the amplitude of the signal, respectively. In both figures the left panel corresponds to the individual neuron, and the right panel, to the coupled neuron. The ISI distribution of the individual neuron has a main peak at the period of the signal, T, which becomes more pronounced as the amplitude of the signal, a_0, increases. When the neuron is coupled to a second neuron that does not perceive the signal, the peak at T becomes broader and less pronounced.

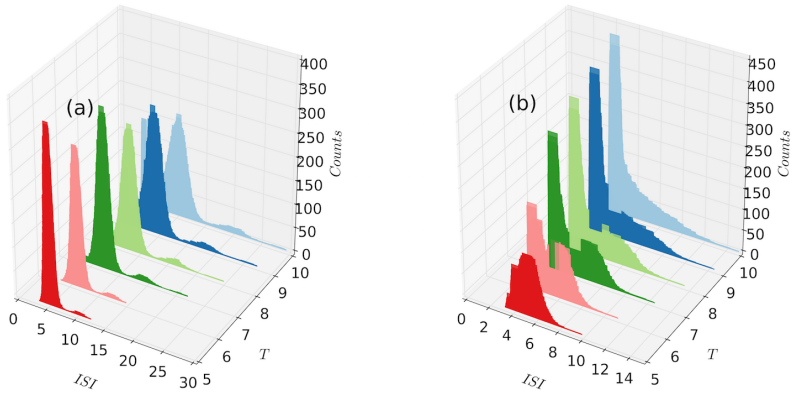

Figure 3.6: Interspike-interval distribution for different periods. The parameters are $a_0 = 0.05$, $D = 2 \cdot 10^{-6}$ and (a) $\sigma = 0$; (b) $\sigma = 0.05$.

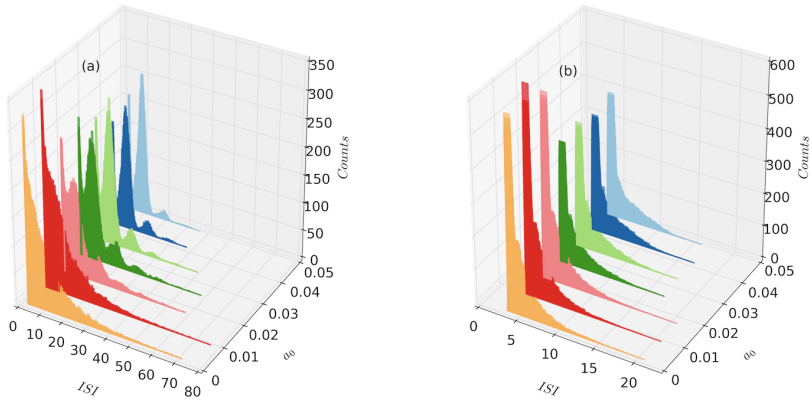

Figure 3.7: Interspike-interval distribution for different modulation amplitudes. The parameters are $T = 10$, $D = 2 \cdot 10^{-6}$ and (a) $\sigma = 0$; (b) $\sigma = 0.05$.

Thus, the coupling to the second neuron tends to wash out the peak, and thus, if the peak encodes the information of the period of the signal, the coupling to neuron 2 degrades the signal encoding.

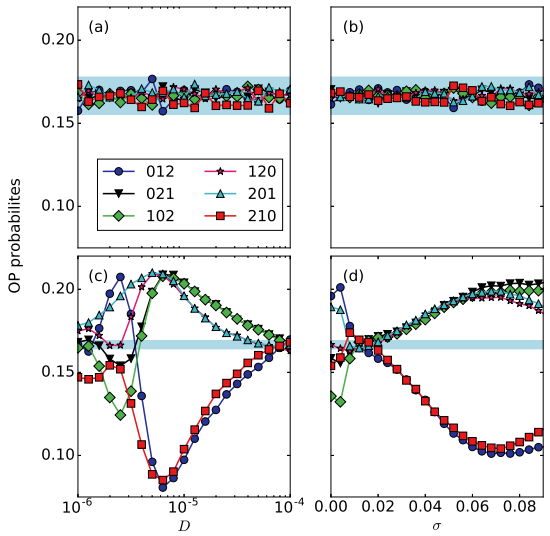

Figure 3.8: Influence of the noise strength and the coupling strength in the ordinal probabilities. In panels (a) and (b) the probabilities of the six ordinal patterns are plotted as a function of D (for $\sigma = 0$) and as function of σ (for $D = 2 \cdot 10^{-6}$), both for $a_0 = 0$. Panels (c) and (d) are as (a) and (b), but a sub-threshold signal is applied ($a_0 = 0.05$ and $T = 10$). In all the panels the blue region indicates the interval of probability values that are consistent with the uniform distribution with 99.74% confidence level.

3.4 Detection and characterization of spike patterns

After having characterized the effects of the weak signal, of the coupling, and of the noise in the neuron's spike rate and in the regularity of the spikes, we next turn our attention to the timing of the spikes. We use symbolic ordinal analysis (see Chapter 2) to investigate the possible presence, in the ISI sequence, of over expressed and of less expressed spike patterns.

We begin by considering the situation in which no signal is applied and analyze the effect of increasing the noise level or the coupling strength: Figs. 3.8 (a) and (b) display the ordinal probabilities as a function of D and σ, respectively. We note that neither the noise nor the coupling induce temporal order in the spike sequence (as all the probabilities are within the blue region that indicates values consistent with equal probabilities). When the signal is applied, panels (c) and (d), we note that there is temporal order in the spike sequence, as the ordinal probabilities reveal the presence of over expressed and less expressed spike patterns (the probabilities are not in the blue region and thus, are not consistent with the uniform distribution). Moreover, we note that the variation of the probabilities with D or σ is qualitatively similar.

Next, we analyze how the coupling coefficients affect the encoding of the signal features (the amplitude and period): we compare how the ordinal probabilities vary with a_0 and T, when neuron 1 is isolated [Figs. 3.9 (a) and (c)] and when it is coupled to neuron 2 [Figs. 3.9 (b) and (d)]. In both cases, when a_0 increases (within the sub-threshold region) the probabilities monotonically increase or decrease. This variation is consistent with the results reported in.[76] While in[76] the sub-threshold signal was applied to the slow variable, v, here it is applied to the fast variable, u. In both cases, the probabilities encode information of the amplitude of the signal. Nevertheless, coupling to neuron 2 changes the preferred and infrequent patters, i.e., modifies the temporal order in the spike sequence. For instance, for $\sigma = 0.05$ the probability of the ordinal pattern 012 monotonically increases with a_0, whereas for $\sigma = 0.05$ monotonically decreases.

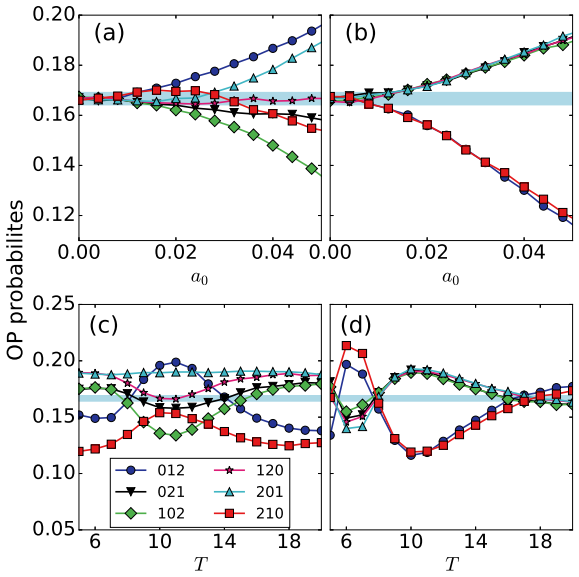

Figure 3.9: Influence of neuron 2 on the encoding of the signal by neuron 1. (a), (b) Ordinal probabilities vs. the signal amplitude, a_0, when the signal period is $T = 10$; (c), (d) probabilities vs. T, when a_0=0.05. Panels (a), (c) are without coupling ($\sigma = 0$), while (b), (d) are with coupling ($\sigma = 0.05$). In all the panels the noise strength is $D = 2 \cdot 10^{-6}$.

In panels 3.9 (b) and 3.9 (d) we note that, with or without coupling, the preferred and infrequent patterns depend on the period of the signal, confirming the results reported in.[76]

Comparing Figs. 3.9 (c) and (d) we note that the coupling can either improve or degrade the signal encoding with respect to the uncoupled situation: for $T = 6$ and $T = 10$ with coupling (panel d) the probabilities have extreme values (maximum or minimum depending of the ordinal pattern), and thus, the coupling enhances the signal encoding. In contrast, for $T \sim 17$ with coupling (panel d) all the probabilities are close to the blue region (while without coupling they are not),

which means that with coupling the probabilities do not encode information of the signal.

Next, we investigate if there is an optimal combination of the signal period, T, and the coupling coefficients, σ_1 and σ_2, for signal encoding. To quantify the information content of the spike train (represented by symbolic ordinal patterns) we calculate the permutation entropy (see Chapter 2).

Figure 3.10 (a), (b) and (c) display the normalized permutation entropy in color code as a function of σ_1 and σ_2 for $T = 6$, $T = 10$ and $T = 14$, respectively.

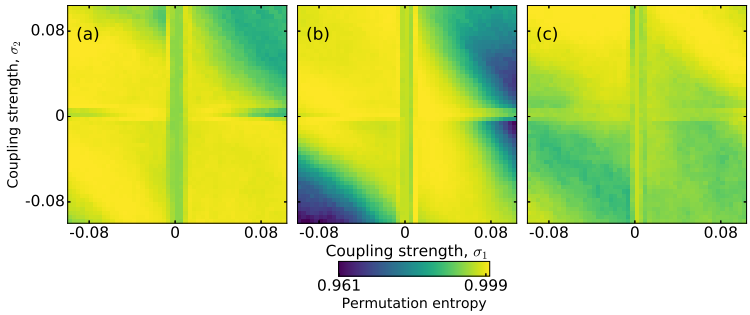

Figure 3.10: Influence of the coupling strengths on the information content of the spike sequence. The information content is quantified by the normalized permutation entropy that is plotted in color code, as a function of the coupling strengths, σ_1 and σ_2, for three periods of the signal: $T = 6$, 10 and 14, panel (a), (b) and (c), respectively. Other parameters are: $a_0 = 0.05$ and $D = 2 \cdot 10^{-6}$.

We observe values very close to 1, which indicate that the timing of the spikes is almost random (the ordinal probabilities are almost equal). This is expected as the signal parameters and the coupling strengths are sub-threshold, i.e., the spiking activity is due to the presence of noise (without noise, the neuron displays sub-threshold oscillations). However, for $T = 10$ (panel b) we see that when $\sigma_1\sigma_2 > 0$ the entropy slightly decreases, which indicates that there are more and less expressed

patterns in the spike sequence, i.e., the spike sequence carries information about the signal.

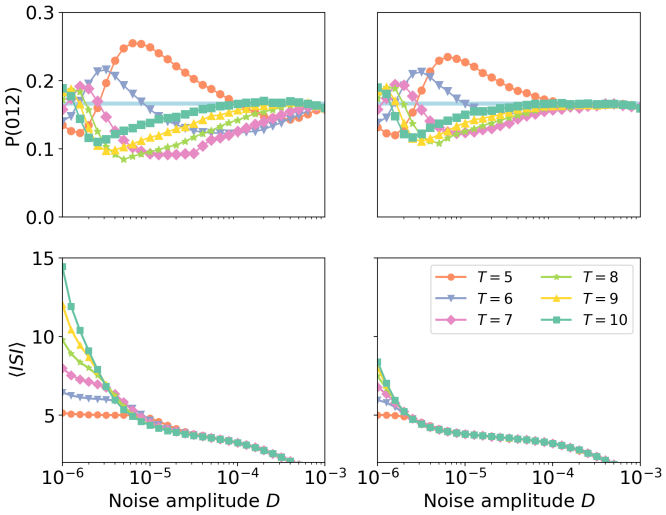

Figure 3.11: Probability of the ordinal symbol 012 in function of the noise amplitude for different modulation periods (see figure inset). (a) 012 ordinal probability for $\sigma = 0$ and for (b) $\sigma = 0.05$. For comparison (c) and (d) display respectively $\langle \text{ISI} \rangle$ for $\sigma = 0$ and $\sigma = 0.05$ for the same modulation periods as in (a) and (b).

It is interesting to compare the results obtained with nonlinear ordinal analysis, with those obtained with linear analysis. Figure 3.11 and 3.12 compare respectively, ordinal pattern probabilities with the mean inter-spike interval and the serial correlation coefficients. Panels 3.11(a) and 3.11(b) display the probability P(012) for neuron 1 and neuron 2 for different periods (see figure inset) as a function of the noise intensity, and panels 3.11(c), 3.11(d) display the corresponding $\langle \text{ISI} \rangle$. We see that, for intermediate and large noise intensities, P(012) depends on the period (i.e. contains information about the period of the signal) while $\langle \text{ISI} \rangle$ does not (is only determined by the level of noise). The $\langle \text{ISI} \rangle$ depends on the period of the

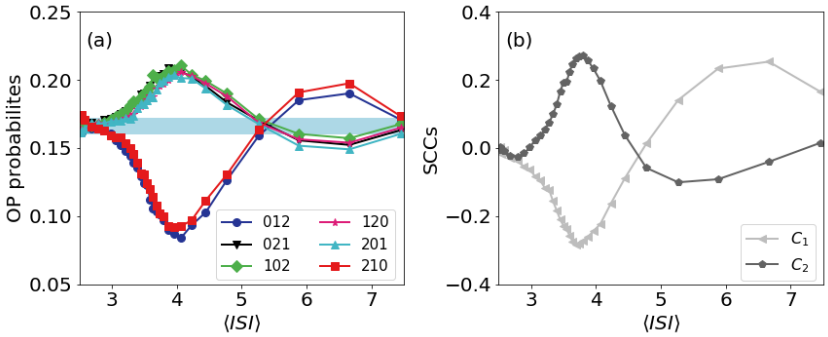

Figure 3.12: (a) Ordinal probabilities and (b) serial correlation coefficients, C_1 and C_2, as a function of the mean ISI, $\langle \text{ISI} \rangle$, when the noise strength is varied within the range $10^{-6} \leqslant D \leqslant 10^{-3}$. Other parameters are $a_0 = 0.05$, $T = 8$, and $\sigma = 0.05$.

signal only for small noise amplitudes (which is reduced for neuron 2).

Linear correlations between inter-spike intervals are detected in Fig. 3.12(b) by the serial correlation coefficients (SCCs, see Chapter 2), where they are plotted vs. the mean ISI, $\langle \text{ISI} \rangle$, which is tuned by changing the noise strength [increasing D decreases $\langle \text{ISI} \rangle$ as shown in Figs. 3.5(a) and (b)]. We see that both measures capture the noise-induced resonance observed by Reinoso and collaborators:[76] both 012 and 210 probabilities reach a minimum when the noise intensity is such that the mean ISI is equal to half of the period (indeed in Fig. 3.12 the period is $T = 8$ and the minimum is observed at $\langle \text{ISI} \rangle = 4$). The same happens with the serial correlation coefficients, for this noise intensity, C_1 is minimum and C_2 undergoes is maximum.

Another relevant issue to discuss is how the coupling terms are implemented. While we have presented model simulations where the terms $\sigma_2 u_1$ and $\sigma_1 u_2$ couple neuron 1 to neuron 2 and vice versa,[110] we have also simulated the model with i)

the coupling in the recovery-like variable (i.e., $\sigma_2 v_1$ and $\sigma_1 v_2$ added to the rate equations of v_2 and v_1 respectively) and ii) with differential coupling (i.e., $\sigma(u_1 - u_2)$ and $\sigma(u_2 - u_1)$ added to the rate equations of u_1 and u_2 respectively).

We have consistently found that the probabilities of the ordinal patterns vary with both, the period and the amplitude of the signal, in a similar way as with non diffusive coupling (see Fig. 3.13). The noise induced-resonance is robust to the type of coupling, panels Fig. 3.13(c) and Fig. 3.13(d) show ordinal patterns probabilities in function of $\langle \text{ISI} \rangle$ for two different periods, $T = 6$ and $T = 8$, respectively. For both periods we observe that both 012 and 210 probabilities are minimum when $\langle \text{ISI} \rangle = \frac{T}{2}$.

3.4.1 Analysis of two coupled non-identical neurons

In order to check the robustness of our findings when the neurons are not identical, we consider two neurons that have different spike rates, which are controlled by the parameters ϵ_1 and ϵ_2, and different spike thresholds, controlled by the parameters a_1 and a_2.

Figure 3.14 displays the ordinal probabilities as a function of modulation period, T, for different values of ϵ_1, while keeping constant ϵ_2 (as in the previous sections, here $\epsilon_2 = 0.01$). We note that the ordinal probabilities depend on the value of ϵ_1 (for example, for large T, patterns 012 and 210 are more expressed for $\epsilon_1 = 0.008$, but they are less expressed for $\epsilon_2 = 0.012$). For higher ϵ_1, the probabilities encode information only if the period T is short, for large T, the probabilities are all in the gray region (consistent with equally probable patterns).

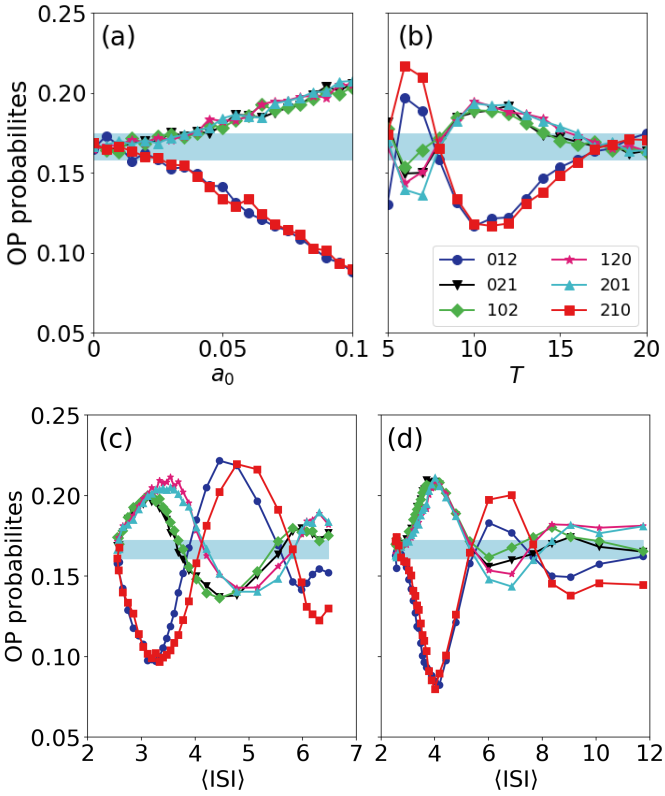

Figure 3.13: Influence of diffusive coupling on the signal encoding. Panels (a) and (b) display the ordinal probabilities as a function of a_0 (with $T = 10$) and as a function of T (with $a_0 = 0.07$). Other parameters are $\sigma = 0.05$ and $D = 5 \cdot 10^{-6}$. Panels (c) and (d) display the ordinal pattern probabilities as a function of the mean ISI when noise strength is varied within the range $10^{-6} \leqslant D \leqslant 10^{-3}$ for $T = 6$ and $T = 8$, respectively. Other parameters are $\sigma = 0.05$ and $a_0 = 0.07$.

In contrast, as seen in Fig. 3.15, the ordinal probabilities remain unchanged when σ_2 is varied in the range 0.005-0.02, while keeping constant ϵ_1 (as in the previous sections, here $\epsilon_1 = 0.01$). One can therefore think that there is no effect of the coupling, however, as Fig. 3.14(c) shows, the ordinal

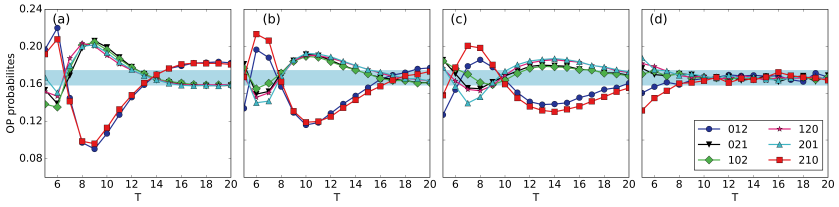

Figure 3.14: Influence of ϵ_1 in the ordinal patterns probabilities. (a) $\epsilon_1 = 0.008$, (b) $\epsilon_1 = 0.01$ (as in the previous sections), (c) $\epsilon_1 = 0.012$ and (d) $\epsilon_1 = 0.02$. The other parameters are $\epsilon_2 = 0.01$, $a_1 = a_2 = 1.05$, $a_0 = 0.05$, $D = 2 \cdot 10^{-6}$ and $\sigma = 0.05$.

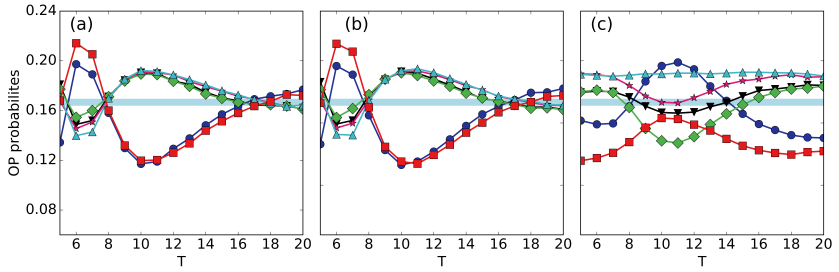

Figure 3.15: Influence of ϵ_2 in the ordinal patterns probabilities. (a) $\epsilon_2 = 0.005$ and (b) $\epsilon_2 = 0.02$. The other parameters are $\epsilon_1 = 0.01$, $a_1 = a_2 = 1.05$, $a_0 = 0.05$, $D = 2 \cdot 10^{-6}$ and $\sigma = 0.05$. In panel (c) the parameters are as in (a) but with $\sigma = 0$.

probabilities are very different when neuron 1 is not coupled to neuron 2.

Similar results are found when changing the values of a_1 and a_2, see Figs. 3.16, 3.17. Taken together our simulations demonstrate that, even when the coupled neurons are not identical, the values of the ordinal probabilities can encode information about period of the weak signal.

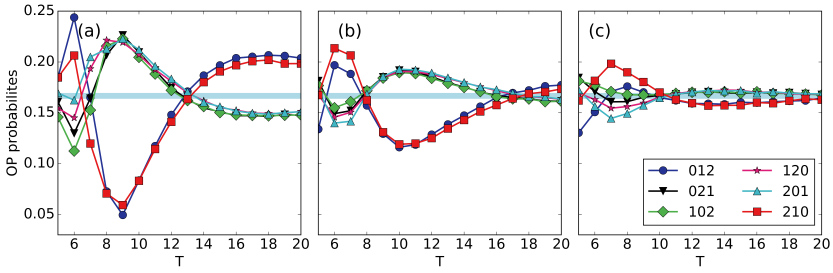

Figure 3.16: Influence of a_1 in the ordinal patterns probabilities. (a) $a_1 = 1.03$, (b) $a_1 = 1.05$ (as in the previous sections), (c) $a_1 = 1.07$ and (d) $\epsilon_1 = 0.02$. The other parameters are $a_2 = 1.05$, $\epsilon_1 = \epsilon_2 = 0.01$, $a_0 = 0.05$, $D = 2 \cdot 10^{-6}$ and $\sigma = 0.05$.

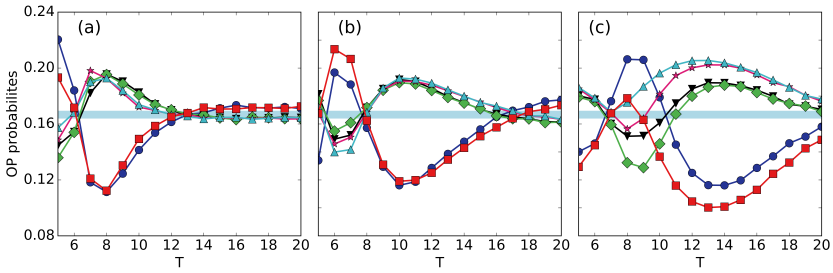

Figure 3.17: Influence of a_2 in the ordinal patterns probabilities. (a) $a_2 = 1.03$, (b) $a_2 = 1.05$ (as in the previous sections), (c) $a_2 = 1.07$. The other parameters are $a_1 = 1.05$, $\epsilon_1 = \epsilon_2 = 0.01$, $a_0 = 0.05$, $D = 2 \cdot 10^{-6}$ and $\sigma = 0.05$.

3.4.2 Signal transmission

So far we have studied how neuron 1 encodes the weak signal when coupled to neuron 2 (which does not perceive the signal). Here, we study how the signal is transmitted to neuron 2 while varying the coupling strength and the modulation period (for a_0 and D fixed) with differential coupling (i.e., $\sigma(u_1 - u_2)$ and $\sigma(u_2 - u_1)$ added to the rate equations of u_1 and u_2 respectively).

Figure 3.18 displays ordinal pattern probabilities and permutation entropy as a function of the coupling strength for $T = 8$ [panels (a), (b) and (c)] and $T = 10$ [panels (d), (e) and (f)]. Panels (a) and (d) display ordinal pattern probabilities for neuron 1, panels (b) and (e) for neuron 2; panels (c) and (f) display the corresponding permutation entropy.

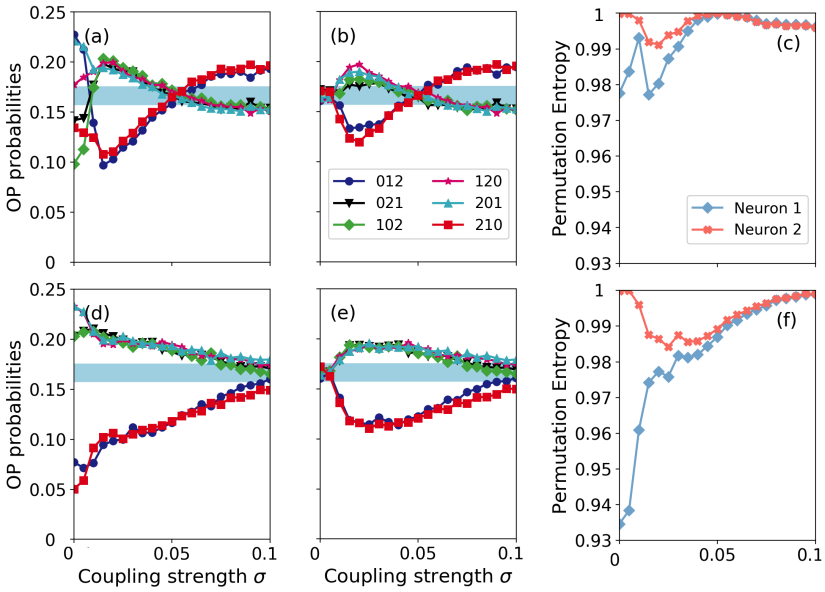

Figure 3.18: Ordinal patterns probabilities for neuron 1 and neuron 2 for $T = 8$, (a) and (b); and for $T = 10$, (d) and (e), respectively. Permutation entropy for neuron 1 and neuron 2 for $T = 8$ (c) and $T = 10$ (f). The other parameters are $a_0 = 0.07$ and $D = 5 \cdot 10^{-6}$.

As the coupling strength increases, neuron 1 transmits the signal to neuron 2 [ordinal patterns probabilities of neuron 2 separate from the equiprobable region, Fig. 3.18(b)]. We quantify this effect by plotting the permutation entropy of neuron 1 and neuron 2 in function of the coupling strength for $T = 8$ [Fig. 3.18 (c)] and $T = 10$ [Fig. 3.18 (f)]. For both periods, permutation entropy of neuron 2 decreases in a cer-

tain range of σ, which indicates that the spikes of neuron 2 are not fully random. As already shown in the previous section, coupling to a second neuron which does not perceive the signal can either improve or deteriorate signal encoding (it depends on the selected parameters D, T and a_0). Here we observe that while for $T = 8$ for some coupling strengths signal encoding improves (permutation entropy of neuron 1 decreases while increasing σ) for $T = 10$, coupling deteriorates it (increasing σ increases permutation entropy). Yet, for both periods (above $\sigma = 0.05$) the ordinal pattern probabilities and the permutation entropy are almost equal for both neurons, suggesting that coupling synchronizes the activity of both neurons. In order to confirm this we compute in Fig. 3.19 the cross-correlation function and the mutual information between neuron 1 and neuron 2 for different modulation periods.

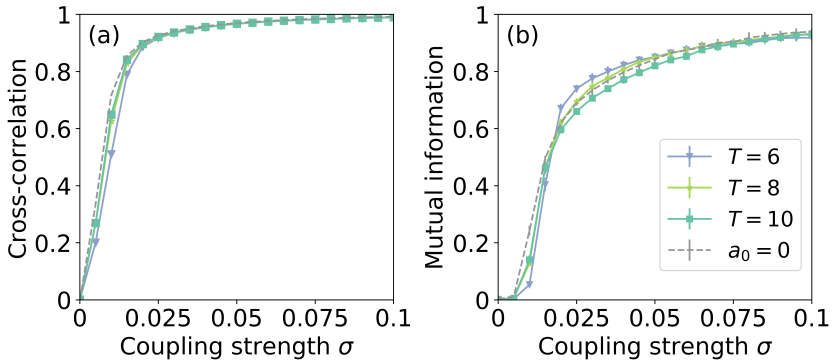

Figure 3.19: Cross-correlation function (a) and mutual information (b) as a function of coupling strength for $a_0 = 0.07$ and different modulation periods (see figure inset), computed also for $a_0 = 0$. For both panels $D = 5 \cdot 10^{-6}$. For the mutual information plot we added errors bars (for most of the values are smaller than the plot markers). We divided the time-series of ordinal patterns into 30 segments, each one of 10000 patterns long, and computed the mutual information with the average for each segment. We computed the error bars as two times the standard deviation of the mean of the mutual information.

As already mentioned in Section 2 the cross-correlation function (Eq. 2.10) captures the linear synchronization between two signals; here we apply it to the time-series of neuron 1 and time-series of neuron 2. It ranges from zero (no synchronization) to 1 (complete synchronization). On the other hand, the mutual information captures the amount of information contained in the time-series of ordinal patterns for neuron 1 and neuron 2 (see chapter 2). Mutual information will range from zero (the random variables are independent between each other, thus not synchronized) from a maximal positive value (they have identical information, thus they are fully synchronized) which equals to the permutation entropy of either neuron 1 or neuron 2. We normalize the mutual information to the maximal value permutation entropy can take $H_{max} = \log L!$ (with $L = 3$).

We observe in Fig. 3.19 that both measures, cross-correlation function and mutual information, capture synchronization between both neurons while increasing σ. The cross-correlation function indicates a strong synchronization already for $\sigma = 0.025$ ($c_{u_1 u_2} \approx 0.98$). Mutual information ranges from zero to a maximum value which is close to the maximal value of the permutation entropy either for neuron 1 or neuron 2 (since we normalize it to the maximal value of the permutation entropy) for that coupling strength, indicating that both sequences of temporal ordinal patterns are similar, thus synchronized. Regarding the cross-correlation function, the period of the signal does not influence synchronization: for the four studied cases, we obtain the same cross-correlation function. On the other hand, mutual information captures small differences that depend on the period, for an intermediate range of coupling strength $0.02 \leqslant \sigma \leqslant 0.075$: in that range we observe slightly different values of the mutual information for $T = 6$ and

$T = 10$. A significance analysis is needed in order to determine the significance of these rather small differences.[101]

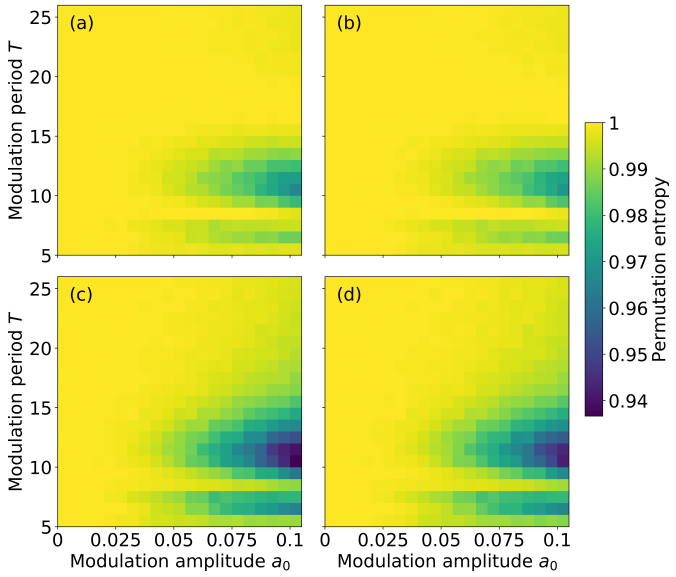

Figure 3.20: Permutation entropy as a function of the modulation period and the modulation amplitude for neuron 1 (panels a, c) and neuron 2 (panels b, d) for $L = 3$ (panels a, b) and $L = 4$ (panels c, d). Other parameters $D = 5 \cdot 10^{-6}$ and $\sigma = 0.05$.

Figure 3.20 displays the permutation entropy for neuron 1 and neuron 2, for $\sigma = 0.05$ and vary both a_0 and T for the same D as in Fig. 3.19. We obtain similar values for neuron 1 and neuron 2 for all a_0 and T suggesting that both neurons are synchronized. As already mentioned in section 2.2.2, the relative order among L consecutive ISI values determines the number of ordinal patterns that we can get. So far, we have only used $L = 3$ and to analyze the robustness of the results, here we also consider L=4.

We observe that the permutation entropy takes smaller values than for $L = 3$, yet the information we obtain either using $L = 3$ or $L = 4$ is the same: (i) for that coupling strength ($\sigma = 0.05$) the signal is transmitted to neuron 2 for all a_0 and T for which neuron 1 encodes the signal and (ii) the signal is encoded for large enough a_0 and for a T which is between the mean ISI and about three times the mean ISI (in the absence of the external signal, and for this level of noise and coupling strength $\langle \text{ISI} \rangle = 5.53$, for both neurons).

3.5 Discussion

We have studied two coupled neurons with a weak periodic signal applied to one of them. We have analyzed how the firing activity of the neuron that perceives the signal encodes the signal information, and the role of another neuron that does not perceive the weak signal. We have shown that when the neuron that perceives the signal is coupled to the second neuron, the spike rate increases and the noise level needed for firing spikes decreases, with respect to the uncoupled neuron. We have used symbolic ordinal analysis to investigate temporal ordering in the timing of the spikes fired by the neuron that perceives the signal. We have shown that the spike sequence has over expressed and less expressed ordinal patterns whose probabilities carry information about the features of the signal (the amplitude and the period). We have also shown that, when the noise is strong, the ordinal probabilities can still encode information about the weak signal, which is not encoded in the spike rate (that is independent of the period of the signal) and is not detected by linear correlation analysis (as the serial correlation coefficients at lags 1 and 2 vanish). We verified that these findings are robust when neurons are

not identical. Finally, we analyzed the activity of the neuron that does not perceive the signal and we have shown that the weak signal is transmitted if the coupling is strong enough. We also quantified signal transmission using linear and nonlinear measures. While both measures captured synchronized behavior with increasing coupling strength, only mutual information seems to detect small differences that depend on the period of the weak signal that is perceived by neuron 1.

Our findings could be relevant for neuronal sensory systems composed by coupled noisy neurons, when only one is affected by external inputs. The encoding and transmission mechanisms demonstrated here, by which the period and the amplitude of the applied sub-threshold signal are encoded in the values of the ordinal probabilities, are very slow if the probabilities are computed from the spike train of a single neuron, because a large number of spikes are needed in order to compute the patterns' probabilities. However, if the encoding is performed by neuronal populations, then, the probabilities can be computed from the spikes of many neurons, and in this case, only few spikes per neuron would be enough to compute the probabilities. This ensemble-based encoding mechanism will be studied in Chapter 5.

Chapter 4

Signal encoding and transmission by two Morris-Lecar neurons

In this chapter we consider two coupled Morris-Lecar neurons and analyze the role of the class of neuronal excitability (class I or II) and the role of the type of coupling: chemical or electrical; birectional or unidirectional. The work presented in this chapter was done in collaboration with Cristian Estarellas and Claudio Mirasso and the results have been accepted for publication in the journal Chaos; a preprint is available in Arxiv.[111] The single neuron Morris-Lecar model was described in Chapter 2. The equations for two coupled neurons with a sinusoidal signal applied to neuron 1 are:

$$\begin{aligned} C\dot{V_1} =& m_\infty(V_1)\cdot g_f\cdot(E_{\mathrm{Na}}-V_1)+W\cdot g_s\cdot(E_{\mathrm{k}}-V_1)+ \\ &+g_l\cdot(E_{\mathrm{l}}-V_1)+a_0\cos(2\pi t/T)+g_{po}+I_1, \end{aligned} \tag{4.1}$$

$$\dot{W_1}=\phi_W\frac{W_\infty(V_1)-W_1}{\tau_W(V_1)}, \tag{4.2}$$

$$C\dot{V}_2 = m_\infty(V_2)\cdot g_f\cdot(E_{\mathrm{Na}}-V_2)+W\cdot g_s\cdot(E_{\mathrm{k}}-V_2) \quad (4.3)$$
$$+\, g_l\cdot(E_{\mathrm{l}}-V_2)+g_{po}+I_2,$$

$$\dot{W}_2 = \phi_W\frac{W_\infty(V_2)-W_2}{\tau_W(V_2)}, \quad (4.4)$$

The parameter I_i refers to the synaptic input (either chemical or electrical) that neuron i receives. The parameters a_0 and T represent the amplitude and period of the external signal and are chosen such that the signal is sub-threshold. The other parameters were defined in chapter 2. As previously stated, we will consider two types of connections, electrical and excitatory chemical synapses. The synaptic input I_i for neuron i due to an electrical synapse is given by,

$$I_i = g_{gap}(V_j - V_i), \quad (4.5)$$

where the electrical conductance g_{gap} regulates its intensity. On the other hand, the synaptic input for neuron i due to an excitatory chemical synapse can be written as

$$I_i = -g_A r_A(V - E_A), \quad (4.6)$$

where E_A is the reversal potential which equals to $E_A = 0$ for excitatory synapses. The parameter g_A is the maximal conductance and scales the magnitude of the input. It is set to obtain a phase locking 1:1 regime between the two coupled neurons: each spike of neuron 1 (that perceives the signal) triggers an spike in neuron 2 (that does not perceive the signal). The variable r_A ranges from $0 \leq r_A \leq 1$ and it represents the probability that a synaptic receptor channel is in an open,

conducting state. This probability depends on the presence and concentration of neurotransmitter released by the presynaptic neuron.[112]

We model its dynamics as in reference:[113]

$$\tau_A \frac{dr_A}{dt} = -r_A + \sum_k \delta(t - t_k), \tag{4.7}$$

The summation over k stands for the pre-synaptic neurons that fired an action potential at time t_k. The time decay is taken as $\tau_A = 5.6$ ms.

We will study the dependency of signal encoding and transmission on neuron's excitability class (class 1 and class 2) and on the synapse's type (electrical or chemical). As well, we are going to consider two types of possible connections, unidirectional and bidirectional, schematically represented in Fig. 4.1 (a) and Fig. 4.1 (b), respectively. They can be either chemical or electrical. In the case of electric coupling, due to the diffusive effect of the gap junction, the more plausible situation is the bidirectional case. However, to compare the two classes of excitability in this study the electrical coupling is used for the unidirectional model as well.

Parameter values

In order to compare excitable class 1 and class 2 neuron types we first analyze how the firing rate of an individual neuron varies with the external noise [Fig. 4.2 (a) and 4.2 (b)]. Whenever we fix the noise intensities, we will use those values that lead to the firing rate of $f_r = 8.6$ Hz. For that firing rate, the noise needed it is neither too strong (it would overtake the dynamics of the system) nor too low (it would not make fire the neurons). For class 1 we will use $g_{p_I} = 6\ \mu\text{S/cm}^2$ and for class

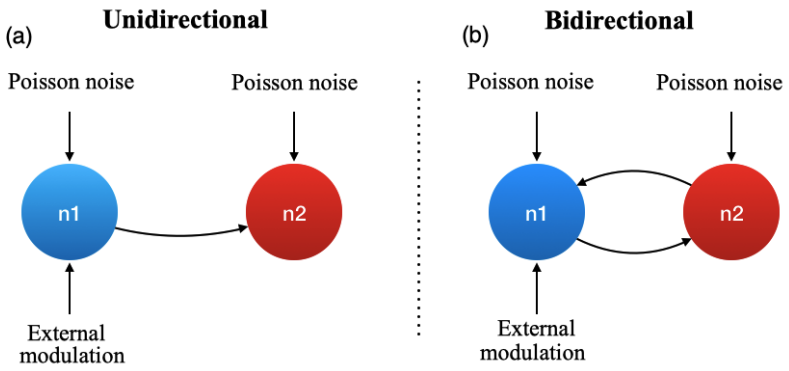

Figure 4.1: Scheme of the unidirectional (a) and bidirectional (b) models. Both neurons receive a Poisson noise but the neuron 1 (blue) also receives an external modulation; neuron 2 (red) is coupled to neuron 1. In the unidirectional case, neuron 1 is coupled to neuron 2.

2 $g_{p_{II}} = 38\ \mu\text{S/cm}^2$. The amplitude of the external signal, a_0 in Eq. 4.2, is normalized such that we have the same signal to coupling ratio in both classes,

$$\frac{a_{0_{m_I}}}{g_{p_I}} = \frac{a_{0_{m_{II}}}}{g_{p_{II}}} = A_0 \tag{4.8}$$

We will vary the normalized modulation amplitude for both neuronal classes from 0 to 2 $\text{mV}/(\mu\text{S/cm}^2)$; it is important to remark that for class 1 neurons the modulation is sub-threshold in the whole range, while for class 2 the signal is supra-threshold for $A_0 \geq 1.625\ \text{mV}/(\mu\text{S/cm}^2)$. Whenever it is fixed, its value will be $A_0 = 1.25\ \text{mV}/(\mu\text{S/cm}^2)$.

Similarly, as it is shown in equation (4.9), the electrical ($g_{gap_{I,II}}$) and chemical ($g_{AMPA_{I,II}}$) conductances are also normalized for both class 1 and class 2 neurons, $g_{gap_{norm}}$ and $g_{AMPA_{norm}}$.

$$\begin{aligned} \frac{g_{gap_I}}{g_{p_I}} &= \frac{g_{gap_{II}}}{g_{p_{II}}} = g_{gap_{norm}} \\ \frac{g_{AMPA_I}}{g_{p_I}} &= \frac{g_{AMPA_{II}}}{g_{p_{II}}} = g_{AMPA_{norm}} \end{aligned} \tag{4.9}$$

Whenever the conductance values are fixed, we take $g_{gap_{norm}} = 50$ (for both unidirectional and bidirectional cases), $g_{AMPA_{norm}} = 83$ (for the unidirectional case) and $g_{AMPA_{norm}} = 50$ (for the bidirectional case). As mentioned before, those parameters lead to a phase locking 1:1 regime between the two coupled neurons.

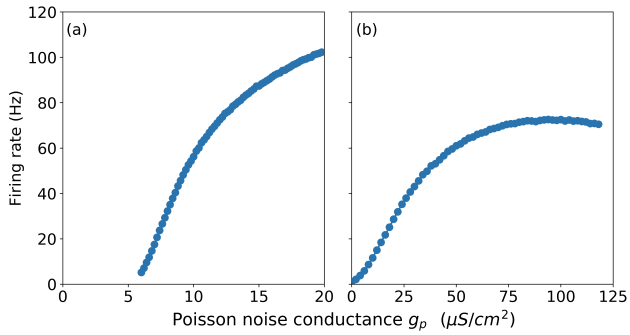

Figure 4.2: Firing rate of neuron 1 (uncoupled and without external modulation) as a function of the synaptic Poisson noise conductance g_p for class 1 (a) and class 2 (b) classes. The constant currents are $I = 14\mu$A and $I = 46\mu$A for class 1 and 2, respectively.

4.1 Signal encoding

In Fig. 4.3 we see that the signal encoding mechanism discussed in Chapter 3 can also occur when the neurons are modeled with the Morris-Lecar model, and it is robust with respect to the coupling type and excitability class.

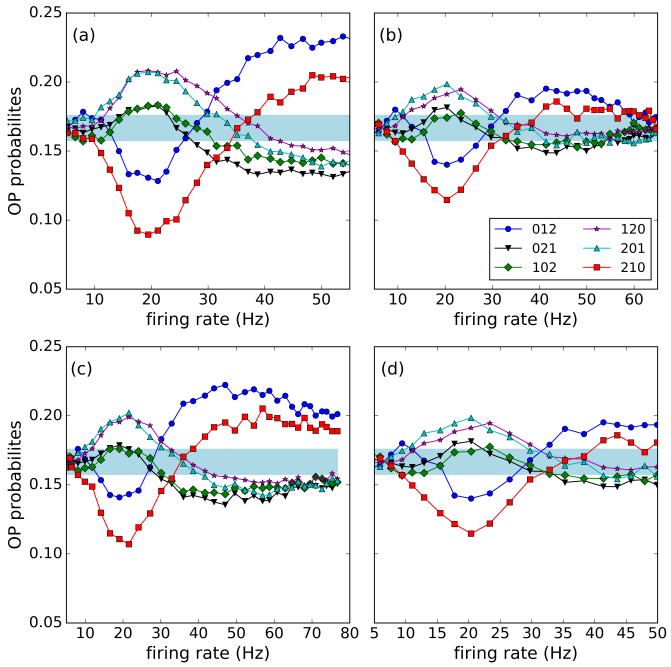

Figure 4.3: Ordinal patterns probabilities as a function of the spike rate for neuron 1 for the bidirectional coupling case. Panels (a) and (b) correspond to class 1 and class 2, respectively, with chemical coupling $g_{AMPA_{norm}} = 50$. Panels (c) and (d) correspond to class 1 and class 2, respectively, with electrical coupling $g_{gap_{norm}} = 50$. Other parameters: $f = 10\ Hz$ and $A_0 = 1.25$ mV/(μS/cm^2). Noise amplitude was within the range 2 μS/cm^2 $< g_p <$ 100 μS/cm^2.

Figure 4.3 displays the ordinal patterns probabilities as a function of the firing rate. In the four panels, we see that the ordinal pattern probability 210 P(210) has a minimum when

the firing rate is close to 20 Hz, twice the value of the applied modulation frequency.

Next, we will quantify information encoding for the unidirectional/bidirectional setting and neuron class by means of the ordinal pattern probabilities and permutation entropy. We will study the encoding of the signal regarding the sequences of spikes of neuron 1. We first consider the unidirectional coupling, which allows us to study signal encoding for a single neuron regarding its excitability class (for the unidirectional set-up, neuron 1 its not coupled to neuron 2). In Fig. 4.4(a) we plot ordinal patterns probabilities of neuron 1 for class 1 in function of the modulation frequency f for a given modulation amplitude A_0. We see that P(012) (blue symbol) exhibits two maxima between $0-10$ and $17-25$ Hz and a minimum between $10-17$ Hz. Thus, the neuron encodes three ranges of external modulation frequencies. Similarly, for the excitability class 2, the neuron encodes three ranges of frequencies [Figure 4.4(c)]. Yet, the encoding is better in class 2 since the difference between the maximal and the minimal ordinal pattern probabilities for a given frequency is larger than for class 1.

In Fig. 4.4(b) we display the permutation entropy of neuron 1 for class 1 while changing the modulation frequency and the modulation amplitude. We observe that the permutation entropy decreases for intermediate frequency signals ($7 \lesssim f \lesssim 22\ Hz$). On the contrary, for class 2 neurons, permutation entropy decreases for high–frequency signals ($f \gtrsim 20\ Hz$), as can be seen in Figure 4.4(d), note that for class 2 neurons for $A_0 \geqslant 1.625\ \frac{\mathrm{mV}}{\mu\mathrm{S/cm^2}}$ the signal becomes supra-threshold, marked with a dotted grey line. However, both classes of neurons start to encode information for a similar minimum amplitude of the external modulation ($A_0 \approx 1\ \frac{\mathrm{mV}}{\mu\mathrm{S/cm^2}}$).

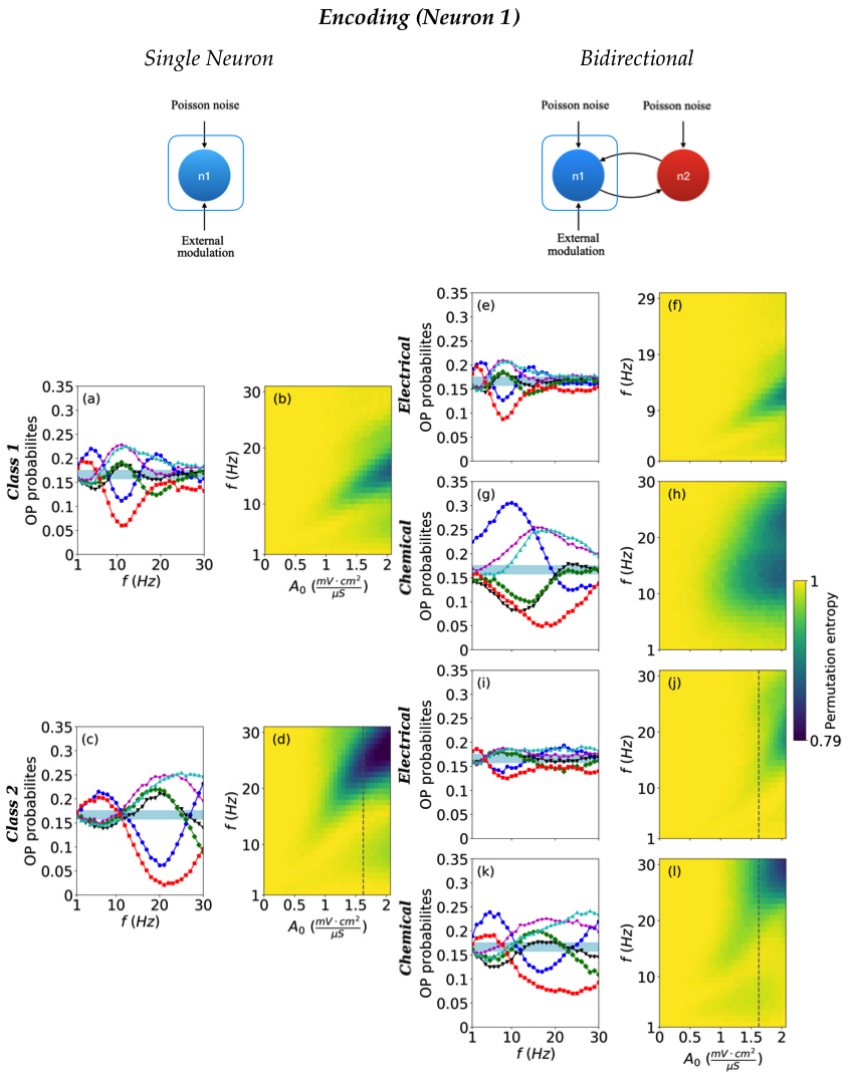

Figure 4.4: Ordinal pattern probabilities vs. the modulation frequency for $A_0 = 1.25$ mV/(μS/cm^2) and permutation entropy in color code as a function of the modulation frequency and the normalized modulation amplitude for neuron 1. (a) and (b) correspond to class 1, (c) and (d) to class 2; the four cases to the single neuron. (e) and (f) correspond to class 1 electrical, (g) and (h) to class 1 chemical, (i) and (j) to class 2 electrical and (k) and (l) to class 2 chemical; all eight panels correspond to the bidirectional coupling. For specific values see section 4.

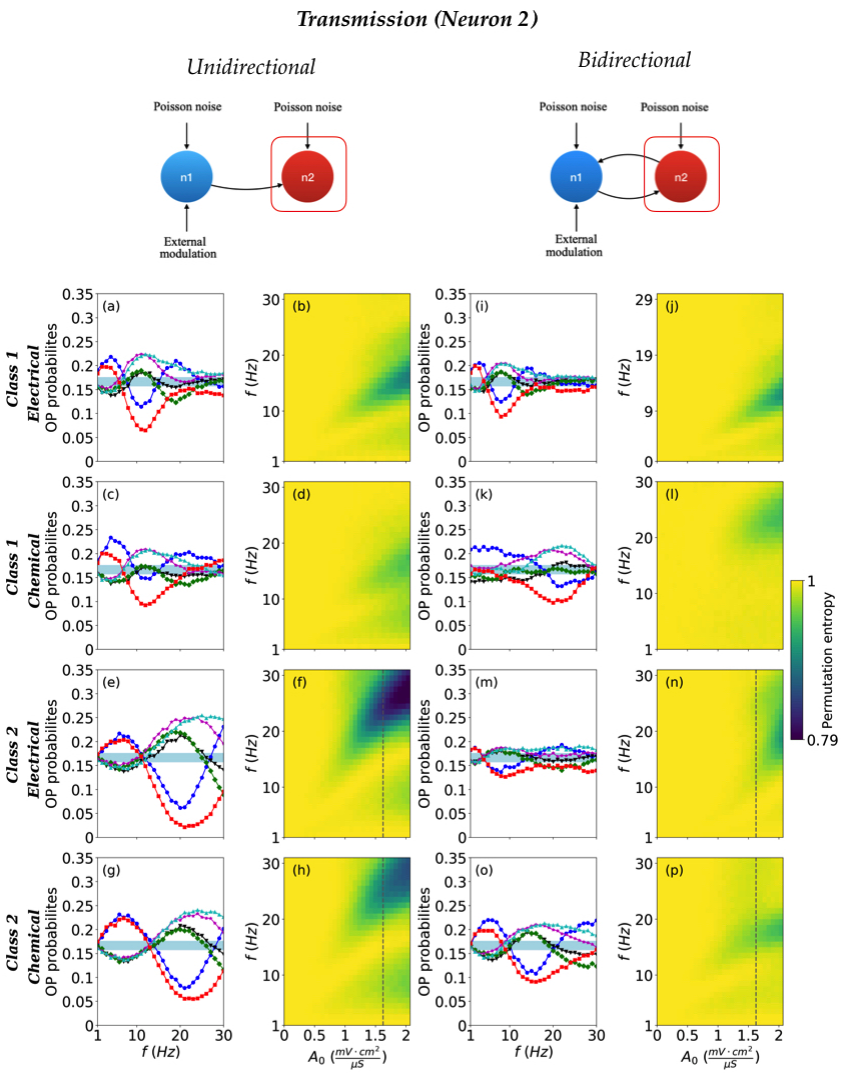

Figure 4.5: Ordinal pattern probabilities vs. the modulation frequency for $A_0 = 1.25$ mV/(μS/cm^2) and permutation entropy in color code as a function of f and a_0 for neuron 2. (a) and (b) correspond to class 1 electrical, (c) and (d) to class 1 chemical, (e) and (f) to class 2 electrical and (g) and (h) to class 2 chemical; the eight cases correspond to unidirectional coupling. (i) and (j) correspond to class 1 electrical, (k) and (l) to class 1 chemical, (m) and (n) to class 2 electrical and (h) and (p) to class 2 chemical; all eight panels correspond to the bidirectional coupling. For specific values see section 4.

Likewise, the permutation entropy decreases gradually as the amplitude increases. A closer look at the permutation entropies and the ordinal pattern probabilities in Fig. 4.4(a), (b) and Fig. 4.4(c), (d) reveals that already small deviation from 1 from the permutation entropy quantify signal encoding. These deviations correspond to the difference between the maximal and minimal ordinal pattern probabilities for a given amplitude and frequency when ordinal patterns probabilities lie outside the equiprobable region (marked as blue).

Next, we study the bidirectional case. In this case the neuron that perceives the external signal is affected by the coupling to the second neuron. Since we have electrical or chemical coupling, we will be able to qualify signal encoding regarding the type of coupling. For the electrical coupling, for class 1 neurons the response of the neuron 1 for the bidirectional system, Fig. 4.4(e), (f) does not have significant differences when compared to the unidirectional case, Fig. 4.4(a), (b). This is reflected in both the ordinal patterns probabilities and the permutation entropy. Thus, electrical coupling for class 1 does not influence signal encoding. On the contrary, for class 2 neurons the bidirectional electrical coupling deteriorates the encoding of the signal [compare Fig. 4.4(c) with Fig. 4.4(i) and Fig. 4.4(d) with Fig. 4.4(j)].

Chemical coupling, for class 1 neurons strongly influences the encoding of the signal, see Fig. 4.4 (g), (h): it changes the preferred and infrequent ordinal patterns, and interestingly it improves the quality of the encoding. In Fig. 4.6(a) we display the spiking dynamics of neuron 1 (blue, top) and neuron 2 (red, bottom) for this particular case: when the best encoding is achieved for $A_0 = 1.25 \ \frac{\mathrm{mV}}{\mu\mathrm{S/cm^2}}$. For comparison, in Fig. 4.6(b) we plot the dynamics for both neurons for the parameters as in panel (a) but without modulation.

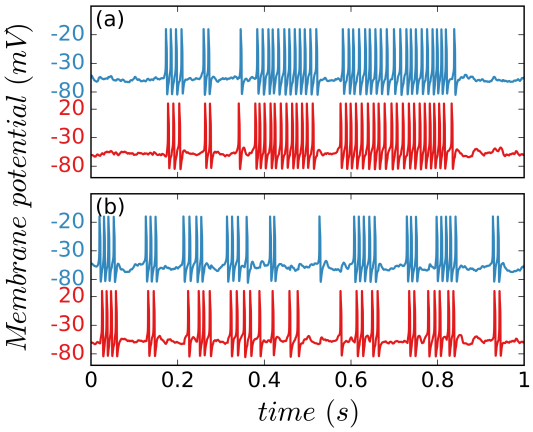

Figure 4.6: Dynamics of neuron 1 (blue, top) and neuron 2 (red, bottom) when (b) the best encoding is achieved when $A_0 = 1.25$ mV/(μS/cm^2) (neuron 1, class 1 and chemical bidirectional coupling; it corresponds to the observed maxima of 012 probability in Fig. 4.5(g) for $f = 10$ Hz). For comparison, panel (a) displays the neurons dynamics for the same parameters as panel (b) without modulation.

On the other hand, for class 2 neurons chemical coupling deteriorates signal encoding: permutation entropy increases on the (A_0, f) plane and the values of the probabilities are closer to the equiprobable region, see Fig. 4.4 (k) and (l).

The effect of chemical coupling for class 1 neurons is characterized in Fig. 4.7 where we display the permutation entropy for neuron 1 (blue line) and neuron 2 (red line) while increasing the chemical coupling: we start with the unidirectional case (neuron 2 is coupled to neuron 1, but not vice versa) and we increase $g_{AMPA_{norm}}$ for neuron 1 until both neurons are bidirectionally coupled. While increasing coupling strength the permutation entropy of both neurons increases, which indicates an increment of stochasticity, meaning that the codification of the signal deteriorates.

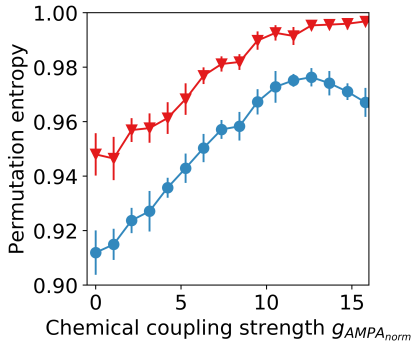

Figure 4.7: Permutation entropy as a function of the chemical coupling strength (bidirectional) for neuron 1 (blue) and neuron 2 (red) for class 2. Parameters: $f = 23$ Hz and $A_0 = 1.25$ mV/(μS/cm^2). The coupling from neuron 1 to neuron 2 is constant ($g_{AMPA_{norm}} = 10$), whereas the conductance $g_{AMPA_{norm}}$ from neuron 2 to neuron 1 increases gradually; going from the unidirectional coupling to totally bidirectional.

4.2 Signal transmission

Here we will study by means of ordinal analysis how the signal is transmitted to the second neuron, i.e., if the ordinal pattern probabilities of neuron 2 are similar to those of neuron 1. We will focus on the influence of the excitability class and type of synapses, electrical and chemical, on signal transmission. While the chemical synapses can be unidirectional or bidirectional, the electrical are mostly bidirectional, although in certain cases a preferred direction for the information flow is established.[114] In any case, both kinds of synapses contribute in a way or another to the communication in the brain.

We first focus on signal transmission for the the unidirectional case. Figures 4.5(a), (c) display ordinal patterns probabilities of neuron 2 in function of the modulation frequency for class 1 for the electrical and chemical synapse, respectively. We observe how neuron 1 transmits the signal regardless of

the coupling type: ordinal pattern probabilities lie outside the equiprobable region. As well, for class 1 and for both couplings ordinal pattern probabilities for neuron 2 vary similarly as for neuron 1 while changing the frequency of the signal [see Fig. 4.4(a)], suggesting that for class 1 and for both unidirectional couplings neurons are synchronized. Yet with electrical coupling we obtain a better transmission and synchronization: ordinal pattern probabilities are further away from the equiprobable region. Comparing Fig. 4.4(b) with Fig. 4.5(b) and Fig.4.5(d), where we display the permutation entropy in the (A_0, f) plane, we observe that this result is also valid for other modulation amplitudes: the darker region in the (A_0,f) plane is really similar for neuron 1 and neuron 2 with electrical coupling.

For class 2 neurons we obtain similar results. If we compare Fig. 4.4(c) with Fig. 4.5(e) and Fig. 4.5(g) we note that the evolution of ordinal pattern probabilities while changing f is almost the same for neuron 1 than for neuron 2 with electrical or chemical coupling. Interestingly, chemical coupling for a certain frequency range ($1 \leqslant f < 15$) improves signal transmission since ordinal pattern probabilities take extremer values compared to neuron 1 and to neuron 2 with electrical coupling. Yet, for the frequency range $15 \leqslant f < 30$ we obtain the best transmission with electrical coupling. This result is also captured in panels 4.4(d), 4.5(f) and 4.5(h), where the permutation entropy is plotted in the plane (A_0, f) for neuron 1, neuron 2 with chemical coupling and neuron 2 with electrical coupling, respectively and for lower frequencies ($f < 15$) chemical coupling transmits better the signal (the permutation entropy takes lower values) while for larger ones $15 \leqslant f < 30$, the electrical synapse does. Figure 4.8(b) displays the spiking dynamics of neuron 1 (blue, top) and neuron 2 (red, bottom)

for the case where the best transmission is achieved (fixing A_0 to 1.25 mv/(μS/cm^2)) for class 2 neurons for a frequency of the external signal $f = 20$ Hz [it corresponds to the minima of 210 probability in Fig. 4.5(g)]. For comparison Fig. 4.6(a) shows the dynamics for both neurons for the same regime as in panel (a) but without modulation.

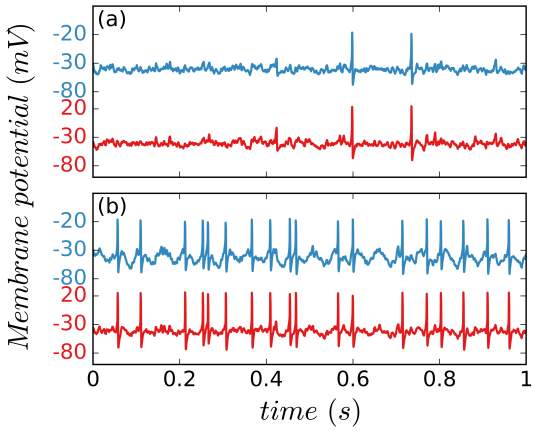

Figure 4.8: Dynamics of neuron 1 (blue, top) and neuron 2 (red, bottom) when (b) the best transmission is achieved when $A_0 = 1.25$ mV/(μS/cm^2) (neuron 2, class 2 and electrical unidirectional coupling; it corresponds to the observed minima of 210 probability in Fig. 4.5(e), for $f = 20$ Hz). For comparison, panel (a) displays the neurons dynamics for the same parameters as panel (b) without modulation.

We proceed with the bidirectional coupling. We observe that ordinal pattern probabilities and permutation entropy for neuron 2 are similar to the ones obtained for neuron 1 with electrical coupling for class 1 [compare panels 4.4(e) and 4.4(f) with 4.5(i) and 4.5(j), respectively] and class 2 [compare panels 4.4(i) and 4.4(j) with 4.5(m) and 4.5(n)], suggesting that electrical coupling synchronizes the activity of both neurons. Yet, for the electrical coupling the best transmission is achieved for class 1, since is for class 1 that we obtain already the best

encoding. Within the same class, if we compare signal transmission regarding coupling type we observe that for class 1 chemical coupling does not transmit the signal [compare panels 4.4(g) with 4.5(k) and 4.4(h) with 4.5(l)]. On the other hand, for class 2 for a given modulation amplitude chemical coupling transmits the signal [compare Fig. 4.4(k) with 4.5(o)]. Nevertheless, if we change A_0 signal transmission for class 2 and chemical coupling its not achieved for all values of f [compare Fig. 4.4(l) with 4.5(p)].

4.3 Discussion

We have studied the neuronal encoding and transmission of a weak periodic external signal using the Morris-Lecar model, which allows us to vary the neuron's excitability class. We have considered two neurons, one that perceives the weak signal and another that does not perceive it. The two neurons interact through different types of coupling (unidirectional or bidirectional, chemical or electrical). To quantify the encoding and the transmission of the signal we have applied symbolic ordinal time series analysis to the sequences of inter-spike-intervals of each neuron. Analyzing the probabilities of symbolic spike patterns, and the permutation entropy computed from the symbolic probabilities, we have studied how information encoding and transmission depend on the excitability class of the neurons, and of the type of connection.

The single neuron class I (class II) encodes low frequencies (higher frequencies) [see Figs. 4.4(b) and 4.4(d)].

When the neurons are class 1, the bidirectional chemical coupling can significantly improve the encoding of the signal. As it can be seen by comparing Figs. 4.4(b) and 4.5(h), the chemical coupling increases the range of frequencies that can be encoded. Instead, the electric coupling has no significant effect in the signal encoding [compare Figs. 4.4(b) and 4.5(f)]. In class 2 neurons, both couplings deteriorate the encoding of the signal, in particular electrical coupling [Figures 4.4(d), 4.4 (j) and 4.4(l)].

Regarding the transmission of the signal, for both excitability classes and connectivity models, electric coupling is the best mechanisms to transmit the information, as the second neuron expresses the symbolic patterns with nearly the same probabilities as the neuron that perceives the signal. Electrical coupling tends to synchronize both neurons due to the diffusive effect from the first neuron to the second one.

In the case of chemical and unidirectional coupling, the information is better transmitted for class 2 neurons [compare Figs. 4.4(d) with Figs. 4.5(d) and Figs. 4.4(d) with Figs. 4.5(h)]. For the bidirectional chemical coupling, neuron 2 does not express the same patterns as those expressed by neuron 1 [for both excitability classes, as seen in Figs. 4.5(l) and 4.5(p)]. Therefore, the information is not properly transmitted.

In general, information transmission is higher with electrical coupling, perhaps due to the fact that electric coupling acts continuously (in contrast, chemical coupling only acts when the neurons fire spikes) due to its diffusive properties. On the contrary, for the case of chemical bidirectional coupling there are changes in the dynamics of both neurons, that potentially provides a new way of encoding the signal features.

Chapter 5

Ensemble of FitzHugh-Nagumo neurons

In this chapter we will investigate if the proposed encoding mechanism (by which preferred and infrequent patterns in the time-series of a neuron carry information about a weak external signal) can be employed by a population of coupled neurons. We consider the stochastic FitzHugh-Nagumo model to simulate the activity of an ensemble of neurons, when they all perceive the weak and periodic signal. The results we present in this chapter are published in.[115] The model equations are:

$$\begin{aligned} \epsilon \dot{u_i} =& u_i - \frac{u_i^3}{3} - v_i + a_0 \cos(2\pi t/T) \\ &+ \frac{\sigma}{k_i} \sum_j^N a_{ij}(u_j - u_i) + \sqrt{2D}\xi_i(t), \qquad (5.1) \\ \dot{v_i} =& u_i + a. \end{aligned}$$

The parameter N refers to the number of neurons. As stated in chapter 2, v_i is the inhibitor variable and u_i is the activator variable of neuron i. The parameters a and ϵ are taken as in chapter 3: $a = 1.05$ and $\epsilon = 0.01$. As in the previous chapters the parameters a_0 and T represent the amplitude

and period of the external signal and are chosen such that the signal is sub-threshold. $D\xi_i(t)$ represents the stochastic term of strength D, which is taken as Gaussian distributed, uncorrelated temporally and across the neuronal ensemble: $\langle \xi_i(t)\xi_j(t')\rangle = \delta_{ij}\delta(t-t')$ with $\langle \xi_i(t)\rangle = 0$ and $\langle \xi_i^2(t)\rangle = 1$.

The neurons are mutually coupled with gap-junction connections, characterized by symmetric links ($a_{ij} = a_{ji} = 1$ if neurons i and j are connected, else $a_{ij} = a_{ji} = 0$). The coupling strength of each link is σ; to keep the total coupling strength uniform for all neurons, it is normalized by number of connections, $k_i = \sum_j a_{ij}$. Regarding the coupling topology, we focus on all-to-all coupling (in this case $k_i = N - 1$ for all i), but we also consider random connections. This allows us to analyze the influence of the number of links, as neurons i and j are connected with probability p that is varied between 0 and 1.

In this chapter, we consider ensembles of up to 50 neurons. We have analyzed the role of the number of neurons, and we expect that our findings will hold for larger ensembles. We will apply ordinal analysis to the sequence of inter-spike intervals generated by the group of neurons. The simulations are done for a time long enough to obtain a total number of 10^5 spikes. Here, we use also $L = 3$. The ordinal pattern probabilities of the ensemble are computed with the sequences of the ordinal patterns of each neuron.

5.1 Influence of the signal's amplitude and frequency

The neuronal ensemble displays different dynamical regimes, depending on the coupling strengh, the signal amplitud and period, the noise strength, and the coupling topology. Figures 5.1 and 5.2 display several examples of the dynamics of a group of 50 neurons under different conditions.

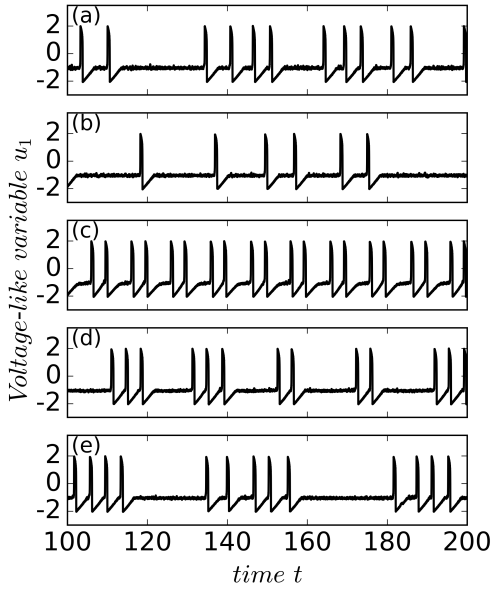

Figure 5.1: Spiking activity of a neuron when no signal is applied ($a_0 = 0$) and the neuron (a) is uncoupled ($\sigma = 0$), (b) is coupled to a group of 50 neurons (all to all coupling, $\sigma = 0.05$). Activity of the neuron when it is coupled and a sinusoidal signal of amplitude $a_0 = 0.1$ and period (c) $T = 10$, (d) $T = 20$, (e) $T = 40$ is applied. The noise level is $D = 2.5 \cdot 10^{-6}$.

Figure 5.1 shows the activity of an individual neuron (the voltage-like variable of neuron 1), while Fig. 5.2 displays the raster plot of the ensemble. In panels 5.1(a) and 5.2(a) the

neurons are uncoupled and no signal is applied, therefore, random spiking activity occurs due to the noise. In panels 5.1(b) and 5.2(b) the neurons are mutually coupled, still no signal is applied. Now we see synchronized spiking activity superposed with random spikes. When the periodic signal is applied, we see in panels 5.1(c)-(f) and 5.2(c)-(f) that the neurons either fire regular and synchronized spikes, or there is more irregular firing, depending on the period of the signal.

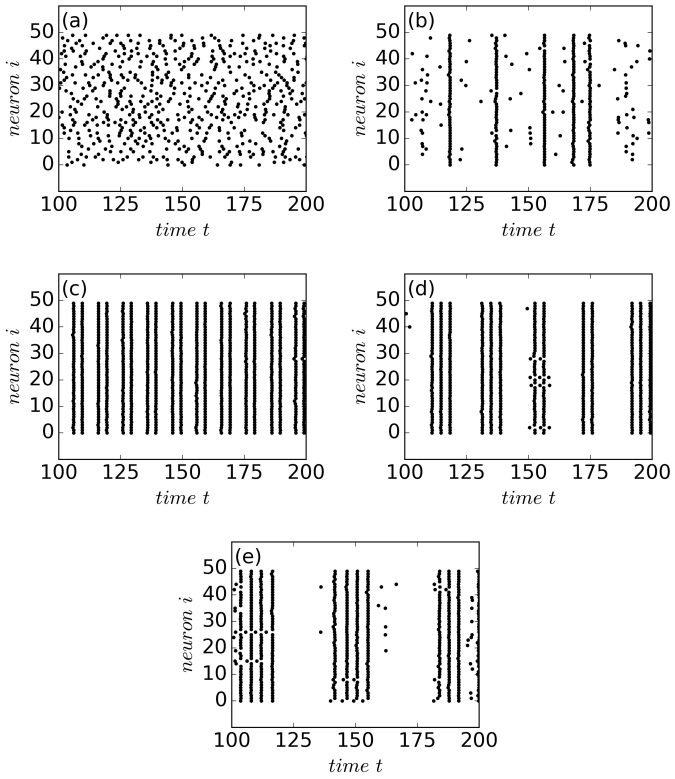

Figure 5.2: Raster plots displaying the spiking activity of the group of 50 neurons for the same parameters as in Fig. 5.1.

In this section we analyze the influence of the amplitude and the period of the modulation. To stress the role of the

number of neurons, we compare the results obtained for 50 neurons with those obtained for only two coupled neurons.

We begin by characterizing the role of the signal amplitude, presented in Fig. 5.3 that displays probabilities of the six ordinal patterns as a function of a_0 for $N = 50$ [Fig. 5.3 (a)] and for $N = 2$ [Fig. 5.3 (b)]. Here a_0 is kept within the range of values for which, in the absence of noise, the neurons do not fire spikes.

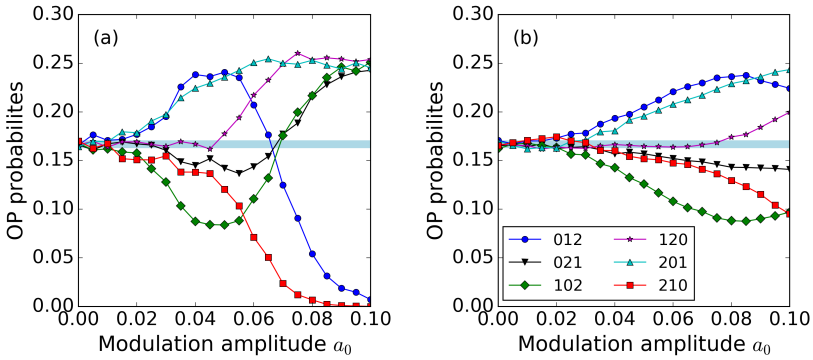

Figure 5.3: Probabilities of the ordinal patterns as a function of the signal amplitude, a_0, for (a) an ensemble of 50 neurons, all-to-all coupled, and for (b) two mutually coupled neurons. The parameters are: $T = 10$, $D = 2.5 \cdot 10^{-6}$ and $\sigma = 0.05$.

We note that, if the signal amplitude is small enough, as expected, the ordinal probabilities are within the blue region that indicates values that are consistent with equal probabilities, with 99.74% confidence level (this region is calculated as explained in chapter 2).

As the signal amplitude increases we note that, while for the two coupled neurons, ordinal probabilities gradually increase (or decrease), for the ensemble of 50 neurons their variation is more pronounced. Interestingly, the same codification (i.e., same ordinal patterns probabilities) is obtained for $N = 2$

and larger a_0. This is shown in Fig. 5.4, where we analyze the effect of the signal period (T is kept within the range of values for which, in the absence of noise, the neurons only display sub-threshold oscillations).

Comparing Figs. 5.4 (a) and 5.4 (d), or Figs. 5.4 (c) and 5.4 (f), we see that for two neurons and larger signal amplitudes we find a very similar set of ordinal probabilities as for 50 neurons and lower a_0. We see that the variation of the ordinal probabilities with the period is very similar for $a_0 = 0.025, N = 50$ and $a_0 = 0.05, N = 2$ [in Figs. 5.4 (a) and 5.4 (d), respectively] and for $a_0 = 0.05, N = 50$ and $a_0 = 0.1, N = 2$ [Figs. 5.4 (c) and5.4 (f), respectively]. Therefore, these results suggest that 50 neurons encode a weak signal in a very similar way as 2 neurons encode a stronger signal.

Regarding how the encoding of the signal depends on its period, in Fig. 5.4 we verify that the probabilities of the patterns expressed in the spike sequences depend on the period of the signal (consistent with the observations in[76,102]). Comparing the left and right columns of Fig. 5.4, we note that neuronal coupling is beneficial for signal encoding because for $N = 50$ (left column) the ordinal probabilities take higher or lower values, and the resonances with the period become more pronounced, as compared to $N = 2$ (right column).

Interestingly, for $N = 50$ and $a_0 = 0.1$ the probabilities are nearly constant in the interval $10 \leq T \leq 15$ and patterns 012 and 210 have very low or zero probability. The corresponding neuronal activity for $T = 10$ was displayed in Figs. 5.1(c) and 5.2(c). We see an alternation of long and short intervals between spikes, while three consecutive increasing or decreasing intervals do not occur (which would be represented by patterns 012 and 210 respectively).

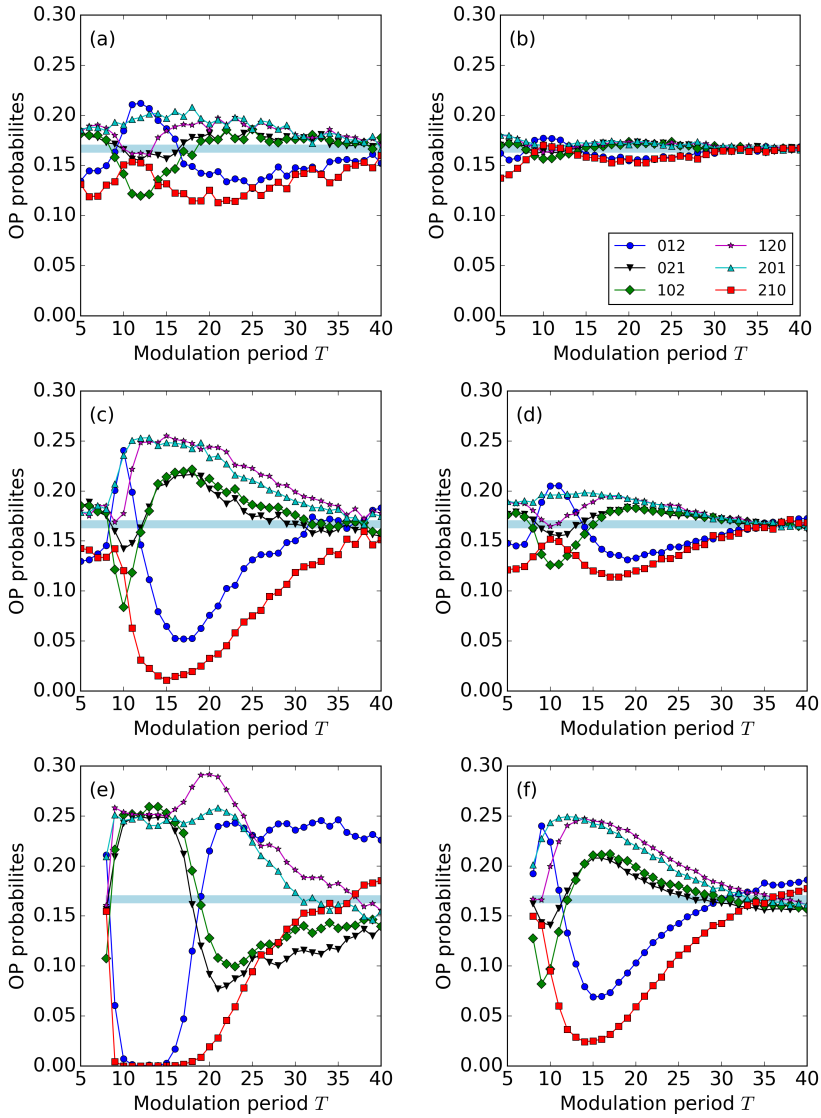

Figure 5.4: Probabilities of the ordinal patterns as a function of the signal period, T, for (a,b) $a_0 = 0.025$, (c,d) $a_0 = 0.05$ and (e,f) $a_0 = 0.1$ with $N = 50$ (a,c,e) and $N = 2$ (b,d,f). In panels (e) and (f) we consider $T \geq 8$ because for $T < 8$ the signal by itself triggers spikes. Other parameters are: $D = 2.5 \cdot 10^{-6}$ and $\sigma = 0.05$.

5.2 Influence of noise strength

In Ref.[76] it was shown that the ordinal patterns displayed a noise-induce resonance, as 012 and 210 reached minimum values when the noise intensity was such that the mean ISI, $\langle ISI \rangle$, was approximately equal to half the signal period. In Ref.[102] it was demonstrated that this encoding mechanism persisted when the neuron was coupled to a second neuron that did not perceive the signal. Here, we show in Fig. 5.5(a) that the mechanism is robust and the resonance is more pronounced when the signal is perceived by a group of 50 neurons: ordinal patterns 012 and 210 are not expressed (have zero probability) when $D = 5 \cdot 10^{-6}$, and for this noise strength, $\langle ISI \rangle = T/2$. For comparison Fig. 5.5(b) shows the ordinal probabilities as a function of D for $N = 2$. Ordinal patterns 012 and 210 are minimum for almost the same noise strength ($D = 8 \cdot 10^{-6}$) which gives $\langle ISI \rangle = T/2$. Yet, the minimum is less pronounced, as compared to the group of 50 neurons.

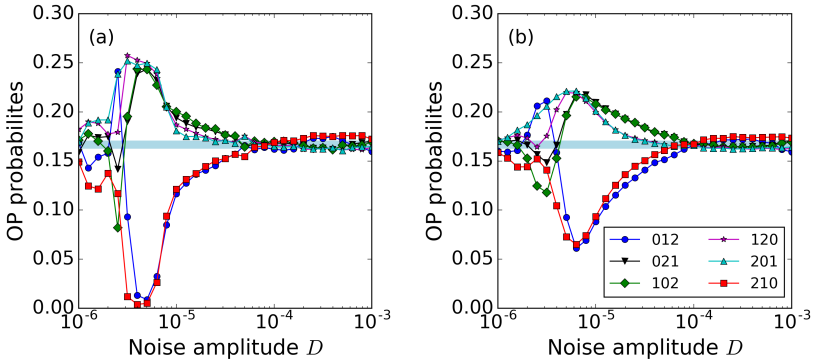

Figure 5.5: Probabilities of the ordinal patterns as a function of the noise strength, D, for (a) 50 neurons and for (b) two neurons. Other parameters are: $a_0 = 0.05$, $T = 10$, and $\sigma = 0.05$.

5.3 Influence of the network structure

So far we have seen that for 50 neurons the encoding of the signal is, in general, improved in comparison with that of only two neurons. Yet, how is the variation of the ordinal probabilities with the network size? Next, we fix the period and the amplitude of the signal and we characterize the influence of i) the number of neurons, N, when they are all-to-all coupled; ii) the number of links (from zero links to all-to-all coupling, randomly adding links) and iii) the strength of the coupling, σ, in the all-to-all configuration, from 0 (uncoupled neurons) to the same coupling strength considered in steps i) and ii). We keep the coupling level low enough such that, without signal and noise, there are no spikes. We note that the starting and final points in the three steps are the same: from the uncoupled neurons to 50 all-to-all coupled neurons.

Figure 5.6 presents the results: panels (a, b) display the ordinal probabilities as a function of N; (c, d) as a function of the percentage of total links; and (e, f) as a function of the coupling strength. To investigate if these parameters can play different roles for weak or strong signals, we consider two signal amplitudes: $a_0 = 0.05$ in panels (a, c, e) and $a_0 = 0.1$ in panels (b, d, f).

In Fig. 5.6(a) we note that for $a_0 = 0.05$ the probabilities gradually vary, increasing or decreasing, as N increases up to $N = 10$. With further increase of N they remain nearly constant. The signal is encoded (the probabilities are not in the blue region) but, at least for these parameters, the encoding only slightly improves when increasing N.

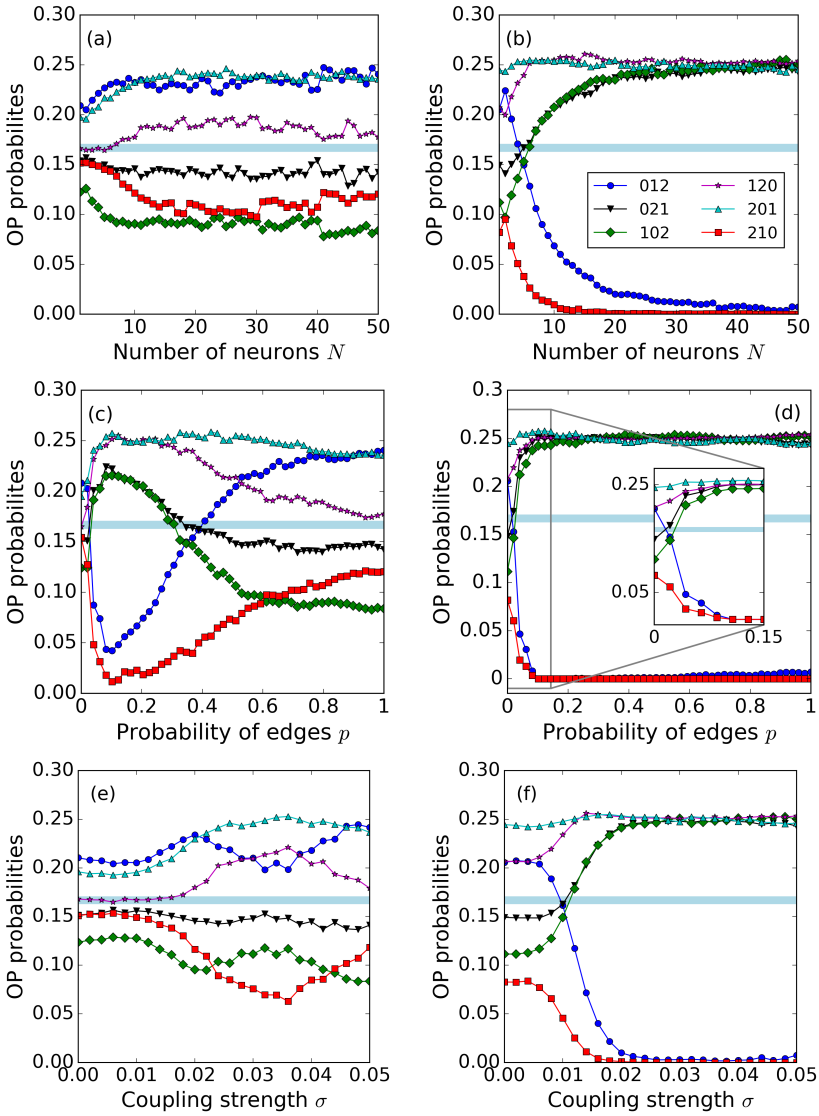

Figure 5.6: Probabilities of the ordinal patterns as a function of the number of neurons, N (a, b), of the percentage of links (c, d), and of the coupling strength (e, f) for $a_0 = 0.05$ and $a_0 = 0.1$, respectively. In panels (a, b, e, f) the neurons are all-to-all coupled, in panels (c, d) the coupling topology is random (starting from uncoupled neurons, links are randomly added until the neurons are all-to-all coupled). In panels (c, d, e, f) $N = 50$, in all the panels: $D = 2.5 \cdot 10^{-6}$ and $T = 10$.

In contrast, for $a_0 = 0.1$ [Fig. 5.6(b)] we observe that the encoding is significantly improved, compared to Fig. 5.6(a), as the probabilities of the ordinal patterns 012 and 210 gradually decrease to zero. An interesting observation is that above a certain number of neurons (which depends on the parameters) the probabilities saturate and remain stable with further increase of N.

In Fig. 5.6(c) and 5.6(d) we note that for the lower signal amplitude, the probabilities vary gradually when increasing the number of links, and with just few links ($\sim$ 10 %) they take the most extreme values, i.e., the encoding is optimal. In contrast, for the higher signal amplitude the probabilities increase or decrease fast, and then saturate. Next, in Fig. 5.6(e) and 5.6(f) we evaluate the effect of the coupling strength. We notice that increasing σ tends to improve the encoding of the signal (the ordinal probabilities tend to higher or lower values), and the effect is more pronounced if the signal amplitude is high. We also note a saturation effect, as for the high signal amplitude, patterns 012 and 210 have zero probability for coupling strengths above $\sigma = 0.02$.

In order to understand the effect of the coupling strength, Fig. 5.7 displays the spiking activity of the neurons for different values of σ. Here we see that when the neurons are uncoupled ($\sigma = 0$) their spiking activity is partially synchronized due to the periodic signal that is perceived by all the neurons. As σ increases, the spikes gradually become even more synchronized. A similar behavior is found (not shown) when the number of existing links increases, keeping σ constant. For future work, it will be interesting to investigate the synchronization transition using synchronization measures based on the ordinal probabilities.[116]

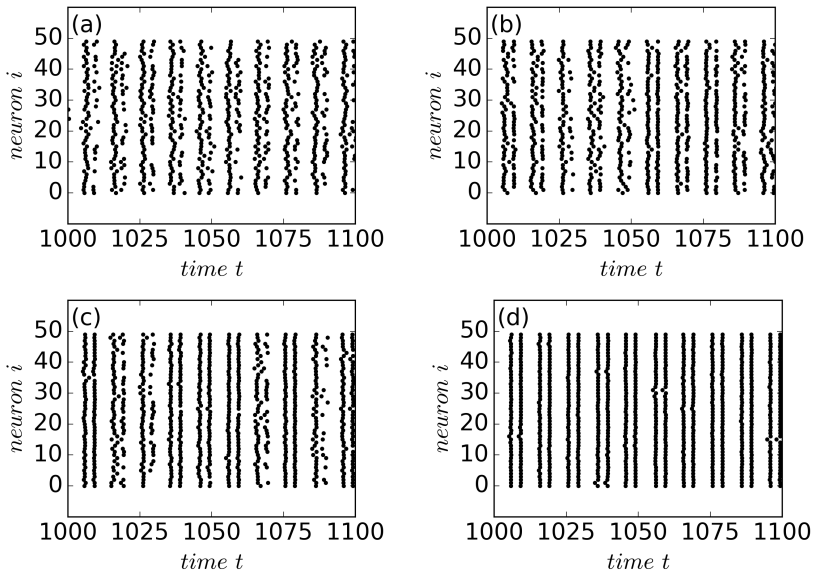

Figure 5.7: Raster plots displaying the spiking activity of the group of 50 neurons all-to-all coupled over time for (a) $\sigma = 0$, (b) $\sigma = 0.01$, (c) $\sigma = 0.015$ and (d) $\sigma = 0.03$. In all the panels: $D = 2.5 \cdot 10^{-6}$, $T = 10$ and $a_0 = 0.1$.

5.4 Discussion

We have analyzed a plausible neuronal mechanism for encoding a weak periodic signal exploiting neural noise. We have simulated the dynamics of a neuronal ensemble using the stochastic FitzHugh-Nagumo model with mutual gap-junction type of coupling, and a sinusoidal signal that is perceived by all the neurons. We applied the ordinal symbolic method to the spike sequences generated by all the neurons. Considering the variation of the ordinal probabilities with the amplitude of the signal, we have found that a group of 50 neurons encodes a weak amplitude signal in a similar way (similar probabilities) as two neurons encode a signal of stronger amplitude.

We confirmed the results reported in Refs.:[76,102] the ordinal probabilities depend on the period and the amplitude of the signal and thus, they encode the signal information. We have found that the probabilities have resonances with the period or with the noise level, which become more pronounced for the neuronal ensemble. Regarding the influence of the number of neurons, N, we have found that increasing N enhances the signal encoding, but above a certain N (which depends on the parameters), the ordinal probabilities saturate and remain nearly constant. We have also investigated the role of the number of links and found that signal encoding can be enhanced by just a few links. We have also found a gradual similar effect when increasing the coupling strength.

In sum, this work concludes that the neuronal ensemble improves signal encoding, in comparison with single or two coupled neurons. We have studied an homogeneous group of neurons as a first step to understand the ensemble coding mechanism.

Chapter 6

Conclusions and Perspectives

6.1 Conclusions

In this thesis we have used well-known neuronal models to analyze the encoding and transmission of weak (sub-threshold) periodic signals. Regarding each chapter, we can summarize the main results as follows.

Signal encoding and transmission by two FitzHugh-Nagumo neurons (Chapter 3)

In this chapter we have demonstrated that the encoding mechanism suggested by Reinoso and collaborators[76] (which states that a weak and periodic signal can be encoded in the probabilities of symbolic spike patterns) is robust to linear coupling and diffusive coupling. It can also hold for non-identical neurons. We have also shown that information extracted using ordinal analysis is complementary to that contained by the analysis of the ISI distribution. Both, the frequency of occurrence of symbolic spike patterns and the ISI distribution can encode the signal information.

The conclusions are:

- If the noise is not too strong ordinal patterns probabilities encode the period of the signal, for both uncoupled and coupled neurons. In contrast, strong noise produces spikes which are too fast, the time interval between spikes is mainly determined by the noise level and therefore the spike sequence does not encode signal's information [Fig. 3.8(c)].

- Coupling can either degrade and enhance signal encoding, depending on the signal parameters [Fig. 3.8(d) and Fig. 3.10].

- Ordinal pattern probabilities encode information of the amplitude of the signal for both coupled and uncoupled neurons: when a_0 increases, the probabilities monotonically increase or decrease [Fig. 3.9(a) and Fig. 3.9(b)].

- For weak noise the mean ISI contains information of the period T of the signal: mean ISI increases with T [Fig. 3.5(c) and Fig. 3.5(d)].

- The coupling to the second neuron increases the width of the ISI distribution (i.e., the variability of the interspike-interval). Therefore, if the signal is encoded in the spike rate, the coupling degrades the encoding of the signal [Fig. 3.6].

- The signal is transmitted to the second neuron if the coupling is strong enough. There seems to be an optimal coupling strength for signal transmission (Fig. 3.18).

Signal encoding and transmission by two Morris-Lecar neurons (Chapter 4)

In this chapter we demonstrated that temporal order in the sequences of spikes is robust to the type of neuronal excitability and synaptic connection. The results are summarized as follows:

- Class 1 neurons are more sensitive to low frequency signals: ordinal pattern probabilities are extremer for lower frequencies [Fig. 4.4(a) and Fig. 4.4(b)]. Class 2 neurons are more sensitive to higher frequencies: ordinal pattern probabilities are extremer for higher frequencies [Fig. 4.4(c) and Fig. 4.4(d)].

- For class 1, bidirectional chemical coupling improves the encoding of the signal: it increases the range of frequencies that neuron 1 can encode [Fig. 4.4(g) and Fig. 4.4(h)]. On the other hand, the bidirectional electric coupling has almost no effect on the range of encoded frequencies. [Fig. 4.4(e) and Fig. 4.4(f)]. For class 2, both bidirectional couplings (chemical and electrical) deteriorate signal encoding, but most notably bidirectional electrical coupling [Fig. 4.4(i), 4.4(j) and 4.4(k), 4.4(l)].

- For the parameters considered, electrical coupling seems to be the best mechanism to transmit information: ordinal pattern probabilities are nearly the same for neuron 2 than for neuron 1, for class 1 and class 2 [Fig. 4.5(a), Fig. 4.5(b), Fig. 4.5(e), 4.5(f), Fig. 4.5(i) and Fig. 4.5(j), Fig. 4.5(m) and Fig. 4.5(n)].

- For chemical coupling the signal is transmitted for all cases except for the bidirectional coupling for class 1:

neuron 2 did not express the same ordinal patterns as neuron 1 [Fig. 4.5(k) and 4.5(l)]. Regarding the other cases, the best signal transmission is achieved for the unidirectional coupling for class 2 [Fig. 4.5(g) and 4.5(h)].

Ensemble of FitzHugh-Nagumo neurons (Chapter 5)

In this chapter we demonstrated that a neuronal ensemble can encode the information of a weak periodic signal in the form of preferred and infrequent symbolic spike patterns, as one and two coupled neurons do. We found that:

- The probabilities of the symbolic spike patterns (i.e., ordinal patterns) depend on both the signal's amplitude and period (Fig. 5.3 and Fig. 5.4).

- Neuronal coupling is beneficial for signal encoding: (i) the neuronal ensemble encodes a weak signal in a similar way as two coupled neurons encode a stronger signal (Fig. 5.3 and Fig. 5.4) and (ii) the neuronal ensemble has extremer resonances with the period of the signal (Fig. 5.4) or with the noise amplitude (Fig. 5.5), in comparison with one or two coupled neurons.

- Few links among the neurons ($\sim$ 10%) are enough to improve signal encoding [Fig. 5.6(c) and Fig. 5.6(d)].

6.2 Future perspectives

- Throughout this thesis we have studied periodic signals. It would be interesting to investigate the encoding and transmission of non periodic inputs, where the amplitude and/or the frequency changes in time.

- We studied how chemical excitatory coupling influenced signal encoding and transmission for two coupled neurons. A more realistic scenario would be to consider a sparse network of coupled neurons with excitatory and inhibitory synapses.

- We analyzed separately the FitzHugh-Nagumo and the Morris-Lecar models, in the future it would be interesting to compare the predictions of these models using parameters for which the relations between the signal period and the mean ISI, as well as the signal amplitude, noise level and coupling strengths are similar.

- We have studied a neuronal ensemble with random coupling topology, however, real neural networks are organized in a modular manner.[117] Thus, we believe that it would be interesting to study the impact of modular organization on signal encoding and transmission. In particular, it would be interesting to study how a signal is encoded by one module and transmitted to the others. On going work is focused in heterogeneous modular networks.

- It would be interesting to analyze how neurons encode two different periodic signals. Chialvo and collaborators[118–120] have shown that *ghost stochastic resonance* occurs in neural systems. When signals with two frequencies are perceived simultaneously, a third frequency is often heard and this is known as *missing fundamental illusion*. Interestingly, ghost stochastic resonance occurs when the frequency that is *absent* is enhanced.

- The study of experimental data (spike trains recorded from biological neurons) is of course needed. There are

freely available datasets, such as the one of Deweese and Zador[121] (where the voltage response to tones of different frequencies from 40 neurons in the primary cortex of a rat is recorded) which would allow for such a comparison. Also, we could compare the synthetic spike sequences of two coupled neurons with other excitable systems, a particular interesting area is the spiking output intensity of two coupled semiconductor lasers with weak external forcing and feedback (in a similar manner Tiana and collaborators[122] did for one semiconductor laser with weak external forcing).

Appendix A

List of publications and research activities

Publications

M. Masoliver, N. Malik, E. Schöll, and A. Zakharova, *Coherence resonance in a network of FitzHugh-Nagumo systems: Interplay of noise, time-delay, and topology*, Chaos **27**, 101102 (2017). Unrelated to this thesis (work done during Master degree at the Tecnische Universität Berlin).

M. Masoliver and C. Masoller, *Sub-threshold signal encoding in coupled FitzHugh-Nagumo neurons*, Sci. Rep. **8**, 8276 (2018).

C. Estarellas, M. Masoliver, C. Masoller and C. Mirasso, *Characterizing signal encoding and transmission in class I and class II neurons via ordinal time-series analysis*, accepted in Chaos (2019). Avaliable at arXiv:1908.01548 (2019).

M. Masoliver and C. Masoller, *Neuronal coupling benefits the encoding of weak periodic signals in symbolic spike patterns*, Communications in Nonlinear Science and Numerical Simulation **82**, 105023 (2020).

Conferences

Jornada d'investigadors predoctorals interdisciplinària. Poster contribution: *Numerical study of the interplay of noise and a subthreshold periodic signal in the output of two coupled neurons.* Barcelona, February, 2017.

International Workshop on Computational Neurosciences and Optical Dynamics. Talk contribution: *Subthreshold signal encoding and transmission in coupled Fitzhugh-nagumo neurons.* Institut de Physique de Nice, Sophia Antipolis, May, 2017.

Crossroads in complex systems conference. Poster contribution: *Interplay of noise and a subthreshold signal in the dynamics of two coupled neurons.* Mallorca, June 2017.

Barcelona Computational, Cognitive and Systems Neuroscience conference (BARCCSYNC). Talk contribution: *Subthreshold signal encoding and transmission in coupled Fitzhugh-nagumo neurons.* Barcelona, June 2017.

17 National Congress of the Spanish Society of Neuroscience. Poster contribution: *Subthreshold signal encoding and transmission in coupled Fitzhugh-nagumo neurons.* Alacant, September 2017.

Deutsche Physicallishes Gesellschaft Conference. Talk contribution: *Coherence resonance in a network of FitzHugh-Nagumo systems: Interplay of noise, time-delay, and topology.* Berlin, March 2018.

Deutsche Physicallishes Gesellschaft Conference. Poster contribution: *Subthreshold signal encoding in coupled FitzHugh-Nagumo neurons.* Berlin, March 2018.

Analysis and Modeling of Complex Oscillatory Systems (AMCOS) Conference. Poster contribution: *Subthreshold signal encoding in coupled FitzHugh-Nagumo neurons.* Barcelona, March 2018.

Barcelona Computational, Cognitive and Systems Neuroscience conference (BARCCSYNC). Poster contribution: *Subthreshold signal encoding in coupled FitzHugh-Nagumo neurons.* Barcelona, May 2018.

VII Jornada complexitat.cat: Complex systems, from theory to data science. Poster contribution: *Characterizing spike sequences generated by different neuronal models via ordinal time-series analysis.* Barcelona, May 2018.

International conference on Mathematical Neuroscience. Poster contribution: *Characterizing spike sequences generated by different neuronal models via ordinal time-series analysis.* Juan les Pins, France, June 2018.

FisEs Conference: XXI Congreso de Física Estadística. Poster contribution: *Information transmission in random and modular neuronal networks.* Madrid, October 2018.

Jornada d'investigadors predoctorals interdisciplinària. Talk contribution: *Information encoding in a neuronal network.* Barcelona, February 2019.

VIII Complexitat Day. Talk contribution: *Information encoding in an ensemble of globally coupled noisy FitzHugh-Nagumo neurons.* Barcelona, May 2019.

Barcelona Computational, Cognitive and Systems Neuroscience conference (BARCCSYNC). Poster contribution: *Neu-*

ronal coupling benefits the encoding of weak periodic signals in symbolic spike paterns. Barcelona, May 2019.

New trends in biomedical imaging and data analysis. Be-Optical Final conference. Talk contribution: *Dynamics of weakly forced excitable systems.* Göttingen, Germany, July 2019.

Workshops and Summer schools

IBERSINC Network congress. Universitat Rovira i Virgili, Tarragona. October 2016.

1rst School Be-optical. Max Plank Institute for Dynamics and Self-organization. November 2016.

VII GEFENOL Summer School on statistical phyisics of complex systems. Institut de física interdisciplinar i sistemes complexes, Universitat de les Illes Balears. 19th - 31th June 2017.

Com millorar l'impacte de la recerca. Gestió de la identitat digital, Universitat Politècnica de Catalunya. Terrassa, 5th July 2017.

IBERSINC Winter school. Universitat Pompeu Fabra. Barcelona, 23th-24th November 2017.

SINC2 one-day workshop on brain connectivity analysis from neural data Entitat organitzadora. Universitat Pompeu Fabra. Barcelona, 23th May 2018.

Summer School UPC-UB. Universitat Politècnica de Catalunya - Universitat de Barcelona. Barcelona, 2nd - 6th July 2018.

Curs de formació del programa educatiu STEAM Barcelona. Universitat de Barcelona, 20th March - 1rst July 2019.

Research stays

Institut de Física interdisciplinar i sistemes complexes, Universitat de les Illes Balears, July 2018 and October 2018. Collaboration with Claudio Mirasso and Cristian Estarellas on the dynamics of two Morris-Lecar Neurons.

Tecnische Universität Berlin. Theoretical Physics. July and August 2019. Collaboration with Anna Zakharova on the dynamics of neuronal networks with multiplex structure.

Teaching

Laboratory of Physics I

- 1rst semester of the academic year 2016-2017.
- 1rst semester of the academic year 2017-2018.
- 1rst semester of the academic year 2018-2019.
- 1rst semester of the academic year 2019-20120.

Laboratory of Physics II

- 2nd semester of the academic year 2016-2017.

Robotic mentor within the educational program STEAM Barcelona. March – June 2019.

Bibliography

[1] E. R. Kandel and A. J. Hudspeth. The brain and behaviour. In *Principles of Neural Science*, pages 5–19. McGraw-Hill, New York, 2012.

[2] G. M. Shepherd. *Foundations of the neuron doctrine*. New York: Oxford University Press, 1991.

[3] J. de Felipe. Cajal y sus dibujos: ciencia y arte. In *Arte y Neurología*. Madrid: Editorial Saned, 2005.

[4] E. M. Izhikevich. *Dynamical Systems in Neuroscience: The Geometry of Excitability and Bursting*. The MIT Press, Cambridge, Massachusetts, London, England, 2010, 2010.

[5] A. Woodruff. Brain anatomy. *The University of Queensland*. https://qbi.uq.edu.au/brain/brain-anatomy.

[6] D. U. Silverthorn. *Human physiology: An integrated approach*. San Francisco: Pearson/Benjamin Cummings, 2007.

[7] S. G. Hormuzdi, M. A. Filippov, G. Mitropoulou, H. Monyer, and R. Bruzzone. Electrical synapses: a dynamic signaling system that shapes the activity of neuronal networks. *Biochimica et Biophysica Acta (BBA) - Biomembranes*, 1662(1):113 – 137, 2004.

[8] P. Dayan and L. F. Abbott. *Theoretical Neuroscience: Computational and Mathematical Modeling of Neural Systems*. Cambridge, US: The MIT press, 2005.

[9] B. Lindner, J. García-Ojalvo, A. B. Neiman, and L. Schimansky-Geier. Effects of noise in excitable systems. *Phys. Rep.*, 392:321–424, 2004.

[10] D. McCormick. Membrane properties and neurotransmitter actions. In *Organization of the Brain*. Oxford University Press, USA, 2004, 2004.

[11] A. L. Hodgkin. The local electric changes associated with repetitive action in a non-medullated axon. *The Journal of physiology*, 107(2):165–181, 03 1948.

[12] A. Longtin, A. Bulsara, and F. Moss. Time-interval sequences in bistable systems and the noise-induced transmission of information by sensory neurons. *Phys. Rev. Lett.*, 67:656–659, 1991.

[13] A. Longtin. Neuronal noise. *Scholarpedia*, 8(9):1618, 2013. revision #137114.

[14] G. Hu, T. Ditzinger, C. Z. Ning, and H. Haken. Stochastic resonance without external periodic force. *Phys. Rev. Lett.*, 71:807, 1993.

[15] L. I. and J.-M. Liu. Experimental observation of stochastic resonancelike behavior of autonomous motion in weakly ionized rf magnetoplasmas. *Phys. Rev. Lett.*, 74:3161–3164, Apr 1995.

[16] A. Longtin. Autonomous stochastic resonance in bursting neurons. *Phys. Rev. E*, 55(1):868, 1997.

[17] A. S. Pikovsky and J. Kurths. Coherence resonance in a noise-driven excitable system. *Phys. Rev. Lett.*, 78:775–778, Feb 1997.

[18] K. Miyakawa and H. Isikawa. Experimental observation of coherence resonance in an excitable chemical reaction system. *Phys. Rev. E*, 66:046204, 2002.

[19] O. A. Rosso and C. Masoller. Detecting and quantifying stochastic and coherence resonances via information-theory complexity measurements. *Phys. Rev. E*, 79:040106(R), 2009.

[20] C. Otto, B. Lingnau, E. Schöll, and K. Lüdge. Manipulating coherence resonance in a quantum dot semiconductor laser via electrical pumping. *Opt. Express*, 22:13288, 2014.

[21] V. Semenov, A. Feoktistov, T. Vadivasova, E. Schöll, and A. Zakharova. Time-delayed feedback control of coherence resonance near subcritical Hopf bifurcation: theory versus experiment. *Chaos*, 25, 2015.

[22] M. Masoliver, N. Malik, E. Schöll, and A. Zakharova. Coherence resonance in a network of fitzhugh-nagumo systems: Interplay of noise, time-delay, and topology. *Chaos: An Interdisciplinary Journal of Nonlinear Science*, 27(10):101102, 2017.

[23] R. Benzi, A. Sutera, and A. Vulpiani. The mechanism of stochastic resonance. *J. Phys. A*, 14:L453, 1981.

[24] A. Longtin. Stochastic resonance in neuron models. *J Stat Phys*, 70:309, 1993.

[25] K. Wiesenfeld, D. Pierson, E. Pantazelou, C. Dames, and F. Moss. Stochastic resonance on a circle. *Phys. Rev. Lett.*, 72:2125–2129, Apr 1994.

[26] J. F. Lindner, B. K. Meadows, W. L. Ditto, M. E. Inchiosa, and A. R. Bulsara. Array enhanced stochastic resonance and spatiotemporal synchronization. *Phys. Rev. Lett.*, 75:3–6, Jul 1995.

[27] K. Wiesenfeld and F. Moss. Stochastic resonance and the benefits of noise: from ice ages to crayfish and squids. *Nature*, 373(6509):33–36, 1995.

[28] Y. Gong, J. Xu, and S. Hu. Stochastic resonance: When does it not occur in neuronal models? *Physics Letters A*, 243(5):351 – 359, 1998.

[29] D. F. Russell, L. A. Wilkens, and F. Moss. Use of behavioural stochastic resonance by paddle fish for feeding. *Nature*, 402(6759):291–294, 1999.

[30] B. Lindner and L. Schimansky-Geier. Coherence and stochastic resonance in a two-state system. *Phys. Rev. E*, 61:6103–6110, Jun 2000.

[31] J. A. Acebrón, A. R. Bulsara, and W.-J. Rappel. Noisy fitzhugh-nagumo model: From single elements to globally coupled networks. *Phys. Rev. E*, 69:026202, Feb 2004.

[32] A. Priplata, J. Niemi, M. Salen, J. Harry, L. A. Lipsitz, and J. J. Collins. Noise-enhanced human balance control. *Phys. Rev. Lett.*, 89:238101, Nov 2002.

[33] L. G. Nowak, R. Azouz, M. V. Sanchez-Vives, C. M. Gray, and D. A. McCormick. Electrophysiological classes of cat

primary visual cortical neurons in vivo as revealed by quantitative analyses. *Journal of Neurophysiology*, 89(3):1541–1566, 2003.

[34] W. Bialek, R. de Ruyter van Steveninck, F. Rieke, and D. Warland. *Spikes. Exploring the Neural Code*. A Bradford Book, 1999.

[35] M. I. Rabinovich, P. Varona, A. I. Selverston, and H. D. I. Abarbanel. Dynamical principles in neuroscience. *Rev. Mod. Phys.*, 78:1213–1265, Nov 2006.

[36] B. Sancristóbal, J. M. Sancho, and J. Garcia-Ojalvo. Phase-response approach to firing-rate selectivity in neurons with subthreshold oscillations. *Phys. Rev. E*, 82:041908, Oct 2010.

[37] R. Krahe and F. Gabbiani. Burst firing in sensory systems. *Nature Reviews Neuroscience*, 5(1):13–23, 2004.

[38] Y. Sakurai. How do cell assemblies encode information in the brain? *Neuroscience & Biobehavioral Reviews*, 23(6):785 – 796, 1999.

[39] D. H. Hubel and T. N. Wiesel. Receptive fields of single neurones in the cat's striate cortex. *The Journal of physiology*, 148(3):574–591, 1959.

[40] D. H. Hubel and T. N. Wiesel. Receptive fields, binocular interaction and functional architecture in the cat's visual cortex. *The Journal of physiology*, 160:106–154, 1962.

[41] D. H. Hubel and T. N. Wiesel. Receptive fields and functional architecture in two nonstriate visual areas (18 and 19) of the cat. *Journal of Neurophysiology*, 28(2):229–289, 1965.

[42] H. Barlow. Grandmother cells, symmetry, and invariance: How the term arose and what the facts suggest. In M.S. Gazzaniga, editor, *The cognitive neurosciences*, pages 309–320. Cambridge, US: The MIT press, 4 edition, 2009.

[43] H. Barlow. The neuron in perception. In M.S. Gazzaniga, editor, *The cognitive neurosciences*, pages 415–434. Cambridge, US: The MIT press, 4 edition, 1995.

[44] H. B. Barlow. Single units and sensation: A neuron doctrine for perceptual psychology? *Perception*, 1(4):371–394, 1972.

[45] C. Blakemore. The language of vision. *New Scientist*, 58(5):674–677, 1973.

[46] S. M. Anstis. What does visual perception tell us about visual coding? In M. Gazzaniga and C. Blakemore, editors, *Handbook of Psychobiology*. New York: Academic Press, 1975.

[47] D. Marr. *Vision: a computational investigation into the human representation and processing of visual information*. Cambridge, US: The MIT press. Originally published in 1982 by W. H. Freeman and Company, 2010.

[48] Churchland P. S. *Neurophilosophy*. Cambridge, US: The MIT press, 1986.

[49] C. G. Gross. Genealogy of the "grandmother cell". *The Neuroscientist*, 8(5):512–518, 2002.

[50] J. Konorski. *Integrative Activity of the Brain: An Interdisciplinary Approach*. Chicago: University of Chicago Press, 1967.

[51] C.D. Salzman, C.M. Murasugi, K.H. Britten, and W.T. Newsome. Microstimulation in visual area mt: effects on direction discrimination performance. *Journal of Neuroscience*, 12(6):2331–2355, 1992.

[52] R. Q. Quiroga, L. Reddy, G. Kreiman, C. Koch, and I. Fried. Invariant visual representation by single neurons in the human brain. *Nature*, 435(7045):1102–1107, 2005.

[53] A. Berkowitz. Population coding. In *Reference Module in Neuroscience and Biobehavioral Psychology*. Elsevier, 2017.

[54] R. Desimone. Face-selective cells in the temporal cortex of monkeys. *J Cognit Neurosci*, 3:1–8, 1991.

[55] C. G. Gross. Representation of visual stimuli in inferior temporal cortex. *Trans R Soc Lond*, 335:3–10, 1992.

[56] A.P. Georgopoulos, A.B. Schwartz, and R.E. Kettner. Neuronal population coding of movement direction. *Science*, 233(4771):1416–1419, 1986.

[57] J. J. Knierim. Chapter 19 - information processing in neural networks. pages 563 – 589, 2014.

[58] R. H. R. Hahnloser, A. A. Kozhevnikov, and M. S. Fee. An ultra-sparse code underliesthe generation of neural sequences in a songbird. *Nature*, 419(6902):65–70, 2002.

[59] A. Amador, Y. Sanz Perl, G. B. Mindlin, and D. Margoliash. Elemental gesture dynamics are encoded by song premotor cortical neurons. *Nature*, 495(7439):59–64, 2013.

[60] N. L. M. Cappaert, N. M. Van Strien, and M. P. Witter. Chapter 20 - hippocampal formation. In G. Paxinos, editor,

The Rat Nervous System (Fourth Edition), pages 511 – 573. Academic Press, fourth edition edition, 2015.

[61] Y Sakurai. Hippocampal and neocortical cell assemblies encode memory processes for different types of stimuli in the rat. *J. Neurosci.*, 16(8):2809, 1996.

[62] C. J. McAdams and J. H. R. Maunsell. Effects of attention on orientation-tuning functions of single neurons in macaque cortical area v4. *Journal of Neuroscience*, 19(1):431–441, 1999.

[63] M. J. Berry, D. K. Warland, and M. Meister. The structure and precision of retinal spike trains. *Proceedings of the National Academy of Sciences*, 94(10):5411–5416, 1997.

[64] D. A. Butts, C. Weng, J. Jin, C. Yeh, N. A. Lesica, J. Alonso, and G. B. Stanley. Temporal precision in the neural code and the timescales of natural vision. *Nature*, 449(7158):92–95, 2007.

[65] B.J. Richmond. Information coding. *Encyclopedia of Neuroscience*, pages 137 – 144, 2009.

[66] Z. F. Mainen and T. J. Sejnowski. Reliability of spike timing in neocortical neurons. *Science*, 268(5216):1503–1506, 1995.

[67] F. Nottebohm. The neural basis of birdsong. *PLOS Biology*, 3, 05 2005.

[68] H. Akolkar, C. Meyer, X. Clady, O. Marre, C. Bartolozzi, S. Panzeri, and R. Benosman. What can neuromorphic event-driven precise timing add to spike-based pattern recognition? *Neural Computation*, 27(3):561–593, 2015.

[69] M. D McDonnell and Lawrence M. W. The benefits of noise in neural systems: Bridging theory and experiment. *Nature Reviews Neuroscience*, 12:415–426, 2011.

[70] A. B. Neiman and D. F. Russell. Models of stochastic biperiodic oscillations and extended serial correlations in electroreceptors of paddlefish. *Phys. Rev. E*, 71:061915, Jun 2005.

[71] W. H. Nesse, L. Maler, and A. Longtin. Biophysical information representation in temporally correlated spike trains. *Proceedings of the National Academy of Sciences*, 107(51):21973–21978, 2010.

[72] A. B. Neiman and D. F. Russell. Sensory coding in oscillatory electroreceptors of paddlefish. *Applied Mathematics and Computation*, 21:047505, 2011.

[73] O. Avila-Akerberg and M. J. Chacron. Nonrenewal spike train statistics: causes and functional consequences on neural coding. *Exp Brain Res*, 210:353–371, 2011.

[74] T. Schwalger and B. Lindner. Patterns of interval correlations in neural oscillators with adaptation. *Frontiers in Computational Neuroscience*, 7:164, 2013.

[75] W. Braun and A. Longtin. Interspike interval correlations in networks of inhibitory integrate-and-fire neurons. *Phys. Rev. E*, 99:032402, Mar 2019.

[76] J. A. Reinoso, M. C. Torrent, and C. Masoller. Emergence of spike correlations in periodically forced excitable systems. *Phys. Rev. E*, 94:032218, Sep 2016.

[77] A. L. Hodgkin and A. F. Huxley. A quantitative description of membrane current and its application to conduction and excitation in nerve. *The Journal of Physiology*, 117(4):500–544, 1952.

[78] E. M. Izhikevich. Which model to use for cortical spiking neurons? *IEEE Transactions on Neural Networks*, 15(5):1063–1070, Sep. 2004.

[79] R. FitzHugh. Impulses and physiological states in theoretical models of nerve membrane. *Biophys. J.*, 1:445, 1961.

[80] J. Nagumo, S. Arimoto, and S. Yoshizawa. An active pulse transmission line simulating nerve axon. *Proc. IRE*, 50:2061–2070, 1962.

[81] E. M. Izhikevich and R. FitzHugh. FitzHugh-Nagumo model. *Scholarpedia*, 1(9):1349, 2006. revision #123664.

[82] C. Morris and H. Lecar. Voltage oscillations in the barnacle giant muscle fiber. *Biophys J*, 35(1):193–213, 07 1981.

[83] H. Lecar. Morris-Lecar model. *Scholarpedia*, 2(10):1333, 2007. revision #151677.

[84] S. H. Strogatz. *Nonlinear Dynamics and Chaos*. Westview Press, Cambridge, MA, 1994.

[85] M. Ciszak, R. Toral, and C. R. Mirasso. Coupling and Feedback Effects in Excitable Systems:. *Modern Physics Letters B*, 18:1135–1155, 2004.

[86] N. Burić, K. Todorović, and N. Vasović. Dynamics of noisy FitzHugh-Nagumo neurons with delayed coupling. *Chaos, Solitons & Fractals*, 40(5):2405–2413, 2009.

[87] G. Ansmann, R. Karnatak, K. Lehnertz, and U. Feudel. Extreme events in excitable systems and mechanisms of their generation. *Phys. Rev. E*, 88:052911, Nov 2013.

[88] Peter Jung, Ann Cornell-Bell, Kathleen Shaver Madden, and Frank Moss. Noise-induced spiral waves in astrocyte syncytia show evidence of self-organized criticality. *J. Neurophysiol.*, 79:1098–1101, 1998.

[89] H. Hempel, L. Schimansky-Geier, and J. García-Ojalvo. Noise-sustained pulsating patterns and global oscillations in subexcitable media. *Phys. Rev. Lett.*, 82:3713–3716, May 1999.

[90] A. Neiman, L. Schimansky-Geier, A. Cornell-Bell, and F. Moss. Noise-enhanced phase synchronization in excitable media. *Phys. Rev. Lett.*, 83:4896–4899, Dec 1999.

[91] B. Hu and C. Zhou. Phase synchronization in coupled nonidentical excitable systems and array-enhanced coherence resonance. *Phys. Rev. E*, 61:R1001–R1004, Feb 2000.

[92] B. Bezekci and V. N. Biktashev. Fast-slow asymptotic for semi-analytical ignition criteria in fitzhugh-nagumo system. *Chaos: An Interdisciplinary Journal of Nonlinear Science*, 27(9):093916, 2017.

[93] I. Efimov, S. Gutbrod, and J. Meyers. 6 - tachycardia termination by shocks and pacing. In *Clinical Cardiac Pacing, Defibrillation and Resynchronization Therapy*, pages 190 – 212. Elsevier, fifth edition, 2017.

[94] S. A. Prescott, Y. De Koninck, and T. Sejnowski. Biophysical basis for three distinct dynamical mechanisms of action

potential initiation. *PLOS Computational Biology*, 4:1–18, 10 2008.

[95] San Miguel M. and Toral R. Stochastic effects in physical systems. In Tirapegui E., Martínez J., and Tiemann R., editors, *Instabilities and Nonequilibrium Structures VI. Nonlinear Phenomena and Complex Systems, vol 5.*, pages 35–127. Springer, Dordrecht, 2000.

[96] C. Bandt and B. Pompe. Permutation entropy: A natural complexity measure for time series. *Phys. Rev. Lett.*, 88:174102, 2002.

[97] J. A. Reinoso, M.C. Torrent, and C. Masoller. Analysis of noise-induced temporal correlations in neuronal spike sequences. *The European Physical Journal Special Topics*, 225:2689–2696, 2016.

[98] O. A. Rosso and C. Masoller. Detecting and quantifying stochastic and coherence resonances via information-theory complexity measurements. *Phys. Rev. E*, 79:040106, 2009.

[99] U. Parlitz, S. Berg, S. Luther, A. Schirdewan, J. Kurths, and N. Wessel. Classifying cardiac biosignals using ordinal pattern statistics and symbolic dynamics. *Compt. Biol. Med.*, 42:319, 2012.

[100] Thomas M. Cover and Joy A. Thomas. *Elements of Information Theory*. Wiley-Interscience, New York, NY, USA, 1991.

[101] G. Lancaster, D. Iatsenko, A. Pidde, V. Ticcinelli, and A. Stefanovska. Surrogate data for hypothesis testing of physical systems. *Physics Reports*, 748:1 – 60, 2018. Surrogate data for hypothesis testing of physical systems.

[102] M. Masoliver and C. Masoller. Sub-threshold signal encoding in coupled fitzhugh-nagumo neurons. *Chaos: An Interdisciplinary Journal of Nonlinear Science*, 8(10):8276, 2018.

[103] B. Lindner, J. García-Ojalvo, A. B. Neiman, and L. Schimansky-Geier. Effects of noise in excitable systems. *Phys. Rep.*, 392:321, 2004.

[104] M. D. McDonnell and L. M. Ward. The benefits of noise in neural systems: bridging theory and experiment. *Physical Review Letters*, 12:415, 2011.

[105] L. Gammaitoni, P. Hänggi, P. Jung, and F. Marchesoni. Stochastic resonance. *Rev. Mod. Phys.*, 70:223–287, 1998.

[106] D. R. Chialvo, A. Longtin, and J. Müller-Gerking. Stochastic resonance in models of neuronal ensembles. *Phys. Rev. E*, 55:1798–1808, 1997.

[107] A. Longtin and D. R. Chialvo. Stochastic and deterministic resonances for excitable systems. *Phys. Rev. Lett.*, 81:4012–4015, 1998.

[108] R. E. Lee DeVille, E. Vanden-Eijnden, and C. B. Muratov. Two distinct mechanisms of coherence in randomly perturbed dynamical systems. *Phys. Rev. E*, 72:031105, 2005.

[109] A.M. Lacasta, F. Sagués, and J.M. Sancho. Coherence and anticoherence resonance tuned by noise. *Phys. Rev. E*, 16:045105, 2002.

[110] R. M. Amro, B. Lindner, and A. B. Neiman. Phase diffusion in unequally noisy coupled oscillators. *Phys. Rev. Lett*, 115:034101, 2015.

[111] C. Estarellas, M. Masoliver, C. Masoller, and C. Mirasso. Characterizing signal encoding and transmission in class i and class ii neurons via ordinal time-series analysis, 2019.

[112] L.F. Abbott and E. Marder. Modeling small networks. In In C. Koch and I. Segev, editors, *Methods in Neuronal Modelling*, pages 361–410. Mit Press, 1998.

[113] V. J. López-Madrona, F. S. Matias, E. Pereda, S. Canals, and C. R. Mirasso. On the role of the entorhinal cortex in the effective connectivity of the hippocampal formation. *Chaos: An Interdisciplinary Journal of Nonlinear Science*, 27(4):047401, 2017.

[114] S. R Robinson, E. C. Hampson, M. N. Munro, and D. I. Vaney. Unidirectional coupling of gap junctions between neuroglia. *Science*, 262(5136):1072–1074, 1993.

[115] M. Masoliver and C. Masoller. Neuronal coupling benefits the encoding of weak periodic signals in symbolic spike patterns. *Communications in Nonlinear Science and Numerical Simulation*, 82:105023, 2020.

[116] I. Echegoyen, V. Vera-Ávila, R. Sevilla-Escoboza, J.H. Martínez, and J.M. Buldú. Ordinal synchronization: Using ordinal patterns to capture interdependencies between time series. *Chaos, Solitons & Fractals*, 119:8 – 18, 2019.

[117] H. Yamamoto, S. Moriya, K. Ide, T. Hayakawa, H. Akima, S. Sato, S. Kubota, T. Tanii, M. Niwano, S. Teller, J. Soriano, and A. Hirano-Iwata. Impact of modular organization on dynamical richness in cortical networks. *Science Advances*, 4(11), 2018.

[118] D. R. Chialvo, O. Calvo, D. L. Gonzalez, O. Piro, and G. V. Savino. Subharmonic stochastic synchronization and resonance in neuronal systems. *Phys. Rev. E*, 65:050902, 2002.

[119] D. R. Chialvo. How we hear what is not there: A neural mechanism for the missing fundamental illusion. *Chaos: An Interdisciplinary Journal of Nonlinear Science*, 13(4):1226–1230, 2003.

[120] Calvo O. and D. R. Chialvo. Ghost stochastic resonance in an electronic circuit. *International Journal of Bifurcation and Chaos*, 16(03):731–735, 2006.

[121] M. R. Deweese and A. M. Zador. Whole cell recordings from neurons in the primary auditory cortex of rat in response to pure tones of different frequency and amplitude, along with recordings of nearby local field potential (lfp). *CRCNS.org*, 2011.

[122] J. Tiana-Alsina, C. Quintero-Quiroz, and C. Masoller. Comparing the dynamics of periodically forced lasers and neurons. *New Journal of Physics*, 21(10):103039, oct 2019.